Stem Cell Reports
Article

ISSCR

OPEN ACCESS

An *EWS-FLI1*-Induced Osteosarcoma Model Unveiled a Crucial Role of Impaired Osteogenic Differentiation on Osteosarcoma Development

Shingo Komura,[1,2] Katsunori Semi,[1,3] Fumiaki Itakura,[1] Hirofumi Shibata,[1] Takatoshi Ohno,[2] Akitsu Hotta,[1,3] Knut Woltjen,[1,4] Takuya Yamamoto,[1,3,5] Haruhiko Akiyama,[2] and Yasuhiro Yamada[1,3,*]

[1]Laboratory of Stem Cell Oncology, Department of Life Science Frontiers, Center for iPS Cell Research and Application (CiRA), Kyoto University, 53 Kawahara-cho, Shogoin, Sakyo-ku, Kyoto 606-8507, Japan
[2]Department of Orthopaedic Surgery, Gifu University Graduate School of Medicine, Gifu 501-1194, Japan
[3]Institute for Integrated Cell-Material Sciences (WPI-iCeMS), Kyoto University, Kyoto 606-8507, Japan
[4]Hakubi Center for Advanced Research, Kyoto University, Kyoto 606-8501, Japan
[5]AMED-CREST, AMED 1-7-1 Otemach, Chiyodaku, Tokyo 100-0004, Japan
*Correspondence: y-yamada@cira.kyoto-u.ac.jp
http://dx.doi.org/10.1016/j.stemcr.2016.02.009

SUMMARY

EWS-FLI1, a multi-functional fusion oncogene, is exclusively detected in Ewing sarcomas. However, previous studies reported that rare varieties of osteosarcomas also harbor *EWS-ETS* family fusion. Here, using the doxycycline-inducible *EWS-FLI1* system, we established an *EWS-FLI1*-dependent osteosarcoma model from murine bone marrow stromal cells. We revealed that the withdrawal of *EWS-FLI1* expression enhances the osteogenic differentiation of sarcoma cells, leading to mature bone formation. Taking advantage of induced pluripotent stem cell (iPSC) technology, we also show that sarcoma-derived iPSCs with cancer-related genetic abnormalities exhibited an impaired differentiation program of osteogenic lineage irrespective of the *EWS-FLI1* expression. Finally, we demonstrate that *EWS-FLI1* contributed to secondary sarcoma development from the sarcoma iPSCs after osteogenic differentiation. These findings demonstrate that modulating cellular differentiation is a fundamental principle of *EWS-FLI1*-induced osteosarcoma development. This in vitro cancer model using sarcoma iPSCs should provide a unique platform for dissecting relationships between the cancer genome and cellular differentiation.

INTRODUCTION

Cancer cells often exhibit similar properties to somatic stem/progenitor cells of the tissue of origin (Reya et al., 2001; Rossi and Weissman, 2006). Considering that progenitor cells at the developmental stage and somatic stem/progenitor cells in some adult tissues have the ability for self-renewal and/or active proliferation, it has been proposed that maintenance of the stem/progenitor cell state could be a driving force for tumor development (Reya et al., 2001). Osteosarcoma is a representative cancer that exhibits shared features with normal stem/progenitor cells (Luo et al., 2008; Thomas et al., 2004). The late markers of osteogenic differentiation are silenced while the early markers are modestly expressed in osteosarcomas (Luo et al., 2008; Thomas et al., 2004). Moreover, more aggressive phenotypes of osteosarcomas are correlated with features of early osteogenic progenitors (He et al., 2010; Luo et al., 2008), suggesting that defects in the osteogenic differentiation program may play a role in osteosarcoma development and progression. However, the causative aberrations that confer stem/progenitor cell properties on osteosarcoma cells are not fully understood.

EWS-FLI1, a widely recognized fusion oncogene for Ewing sarcomas, is generated by the chromosomal translocation of t(11;22) (q24;q12), which consists of the N-terminal transactivator domain of the *EWS* gene and the C-terminal ETS DNA binding domain of the *FLI1* gene. The resulting EWS-FLI1 fusion protein harbors multiple functions, acting as a transcriptional activator, transcriptional repressor, chromatin modulator, and splicing modulator (Kinsey et al., 2006; Riggi et al., 2014; Selvanathan et al., 2015; Smith et al., 2006). Despite the variety of oncogenic functions of *EWS-FLI1*, a number of previous studies implied that *EWS-FLI1* expression itself is not sufficient to induce Ewing sarcoma (Lin et al., 2008; Miyagawa et al., 2008; Riggi et al., 2008; Tanaka et al., 2015) and that other aberrations may be necessary. Indeed, genetic variants near *EGR2* and *TARDBP* are associated with susceptibility to Ewing sarcoma (Grunewald et al., 2015; Postel-Vinay et al., 2012). Moreover, additional genetic mutations, such as *TP53*, *CDKN2A*, and *STAG2*, have been identified in a subset of Ewing sarcomas (Crompton et al., 2014; Tirode et al., 2014). However, it remains unclear whether these mutations are additional driver mutations or passenger mutations and how they contribute to the sarcoma development.

The derivation of induced pluripotent stem cells (iPSCs) demonstrated that mammalian somatic cells can be reprogrammed into pluripotent stem cells (Takahashi and Yamanaka, 2006). It is noteworthy that the reprogramming process does not require any particular alterations to the

genetic information, which makes iPSC technology suitable to study the genotype-phenotype relationship in various diseases (Soldner et al., 2009; Yamashita et al., 2014). Considering that cancer is a genetic disease involving genetic mutations, single nucleotide variants, and structural abnormalities of the chromosome, iPSCs derived from cancer cells are expected to harbor shared genetic abnormalities with the parental cancer cells and therefore should be a powerful tool for dissecting the role of the cancer genome on the phenotype (Semi and Yamada, 2015).

Here, we established a murine *EWS-FLI1*-induced osteosarcoma model from adult bone marrow stromal cells using a doxycycline (Dox)-inducible-*EWS-FLI1* expression system. We revealed that *EWS-FLI1* expression inhibits the osteogenic differentiation of sarcoma cells in vitro and in vivo. Moreover, we found that iPSCs derived from the *EWS-FLI1*-induced osteosarcoma cells exhibit impaired osteogenic differentiation and give rise to sarcoma cells after osteogenic differentiation in vitro in conjunction with *EWS-FLI1* expression.

RESULTS

Establishment of *EWS-FLI1*-Inducible ESCs and Mice

First, we tried to establish an *EWS-FLI1*-inducible mouse model with locus targeting methods. We established two transgenic systems using embryonic stem cell (ESC) lines containing Dox-inducible *EWS-FLI1* alleles that were integrated at different loci by utilizing the KH2 system and *Rosa26* targeting vector (Figures 1A, S1A, and S1B) (Ohnishi et al., 2014; Yamada et al., 2013; Beard et al., 2006). In both ESC lines, reverse tetracycline-controlled transactivator (rtTA) is expressed from the *Rosa26* locus, and the Tet operator-*EWS-FLI1-ires-mCherry* construct is integrated into either the 3′UTR of the *Col1a1* locus (*Rosa-M2rtTA/Col1a1*::*tetO-EWS-FLI1*) or *Rosa26* locus (*Rosa-M2rtTA/Rosa*::*tetO-EWS-FLI1*). Both ESCs expressed mCherry fluorescence upon treatment with Dox in vitro (Figure 1B). The inducible *EWS-FLI1* expression in ESCs was also confirmed by qRT-PCR and western blotting (Figure 1C).

Next, we performed blastocyst injection of *EWS-FLI1*-inducible ESCs and obtained chimeric mice (Figure 1D and Table S1). Upon Dox treatment, *EWS-FLI1* was expressed in a wide variety of organs and tissues of the mice, including the bone marrow and the cortex of the bone where Ewing sarcomas often arise (Figures 1E, 1F, and S1C). Some mice (*Rosa-M2rtTA/Col1a1*::*tetO-EWS-FLI1*) died soon after *EWS-FLI1* induction, which was accompanied by dysplastic changes of intestinal cells due to impaired differentiation (8 of 14 mice, Figures 1G and S1D). However, despite the long-term induction of *EWS-FLI1* (up to 13 months), we did not observe any *EWS-FLI1*-dependent tumor formation in either system (Figure 1G).

Establishment of *EWS-FLI1*-Dependent Immortalized Cells with the Dox-Inducible *EWS-FLI1* Lentiviral System

Our results suggested that the induction of *EWS-FLI1* in adult mice is not sufficient for sarcoma development. Indeed, there is no report that shows the generation of *EWS-FLI1*-driven sarcomas by the targeted insertion of *EWS-FLI1* except for one study that reported the development of myeloid/erythroid leukemia (Torchia et al., 2007). However, previous studies have succeeded in modeling Ewing-like sarcomas in mice when combined with *Trp53* deletion or an integrating viral delivery system with the *EWS-FLI1* fusion gene, which is consistent with the hypothesis that additional genetic mutations may be required for *EWS-FLI1*-induced sarcoma development (Castillero-Trejo et al., 2005; Lin et al., 2008; Riggi et al., 2005; Tanaka et al., 2014).

Accordingly, we generated a lentiviral *EWS-FLI1* expression vector with the Dox-inducible expression system (Figure 2A). A *TetO-EWS-FLI1-ires-Neo* cassette was lentivirally transduced into bone marrow stromal cells from adult *Rosa26-M2rtTA/M2rtTA* mice (3–4 weeks of age). The transduced bone marrow cells were cultured with Dox and G418. The surviving cells were subsequently cultured for 2 months in culture medium containing Dox and G418. Although most cells with *EWS-FLI1*-inducible alleles did not survive, we nevertheless obtained three immortalized cell lines (EFN#2, EFN#12, and EFV#4; Figure 2B). The three lines expressed *EWS-FLI1* mRNA and protein in response to Dox (Figures 2C and 2D) and continuously proliferated under the Dox-containing culture condition (Figure 2B). Upon the withdrawal of Dox, the morphology of two cell lines (EFN#2 and EFN#12) gradually changed to a flat shape and proliferation was inhibited, whereas the third cell line (EFV#4) did not show any evidence of Dox dependency in terms of cellular kinetics (Figure S2A). These observations show that we obtained two *EWS-FLI1*-dependent immortalized cell lines from murine adult bone marrow stromal cells in vitro.

EWS-FLI1-Dependent Immortalized Cells Formed Osteosarcomas In Vivo

To confirm whether the *EWS-FLI1*-dependent immortalized cell lines have tumorigenic potential in vivo, we transplanted EFN#2 and EFN#12 into the subcutaneous layer of immunocompromised mice. At 10 weeks after the inoculation, the transplanted mice developed tumors from both cell lines when they were given Dox (16/16 for EFN#2, 2/4 for EFN#12; Figures 2E and 2F), whereas no tumor

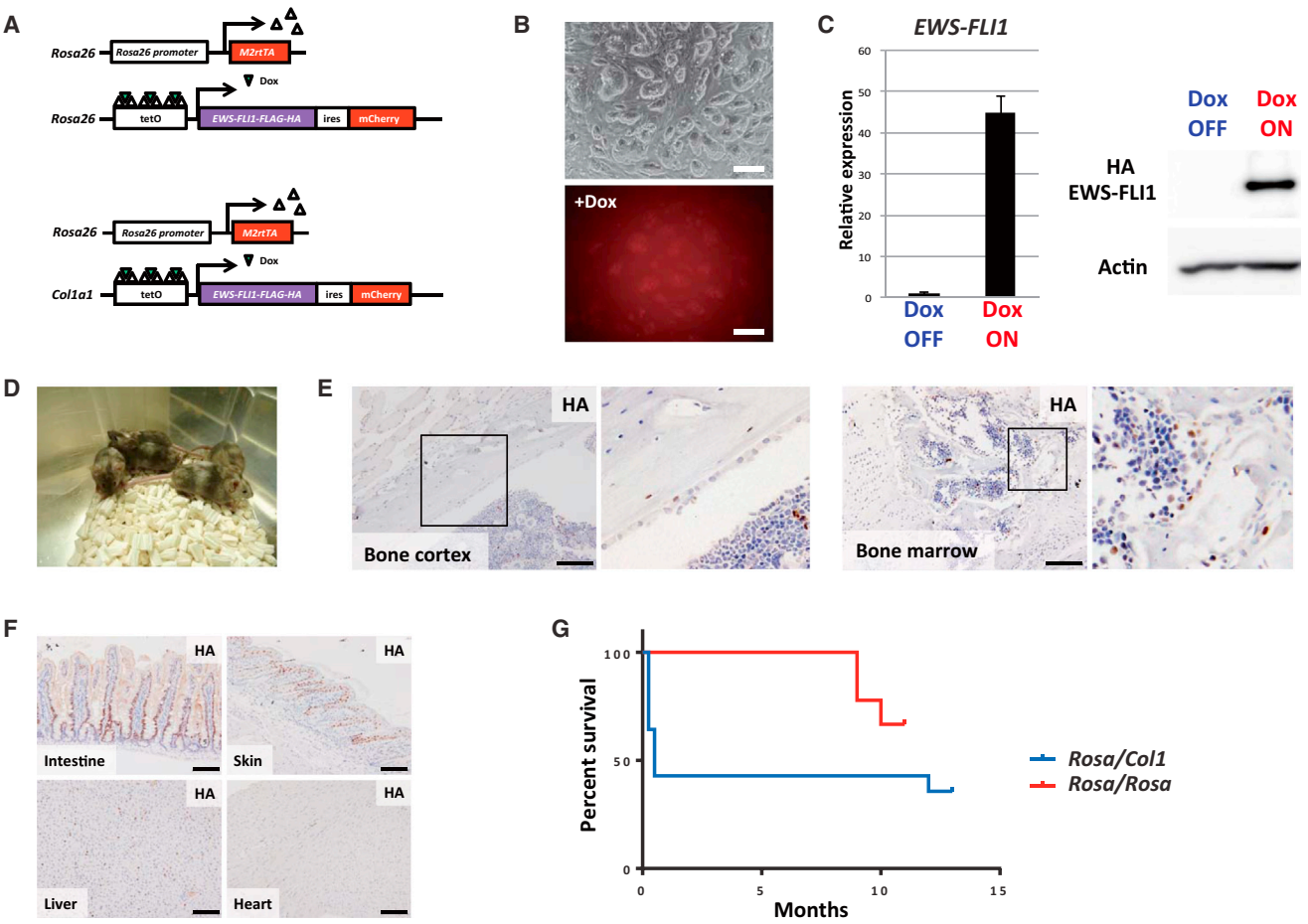

Figure 1. ESCs and Chimeric Mice with the Dox-Inducible *EWS-FLI1* Expression System

(A) Schematic illustrations of the Dox-inducible *EWS-FLI1* expression system. Two distinct ESC lines with Dox-inducible *EWS-FLI1* expression alleles targeted at different loci were established. Upward triangles (white), rtTA; downward triangles (green), Dox.

(B) *EWS-FLI1*-inducible ESCs (*Rosa-M2rtTA/Col1a1*::*tetO-EWS-FLI1-ires-mCherry*). The mCherry signal was detectable upon Dox exposure for 24 hr. Top, bright field; bottom, mCherry. Scale bars, 200 μm.

(C) *EWS-FLI1* mRNA and protein are detectable in ESCs upon Dox exposure for 24 hr. Data are presented as means ± SD (three technical replicates). The expression level of Dox OFF cells was set to 1. Similar results were obtained in both ESC lines.

(D) Chimeric mice were generated by injecting *EWS-FLI1*-inducible ESCs into blastocyst.

(E) Immunohistochemistry of various organs of chimeric mice treated with Dox for 2–7 days. Anti-HA antibody was used to detect EWS-FLI1 fusion protein. EWS-FLI1-positive cells are observed in the bone cortex and the bone marrow after treatment with Dox. Scale bars, 100 μm.

(F) EWS-FLI1-positive cells were observed in various organs after treatment with Dox. Scale bars, 100 μm.

(G) *EWS-FLI1* expression failed to generate sarcomas in chimeric mice derived from two ESCs. Some *Rosa-M2rtTA/Col1a1*::*tetO-EWS-FLI1* mice died in the early phase, presumably because of a gastrointestinal disorder (Figure S1D). Some mice died in the late phase because of *EWS-FLI1*-independent spontaneous cancer development such as lymphoma and lung cancer. *Rosa-M2rtTA/Col1a1*::*tetO-EWS-FLI1* mice, n = 14; *Rosa-M2rtTA/Rosa*::*tetO-EWS-FLI1* mice, n = 9.

formation was observed in mice without Dox administration (0/16 for EFN#2, 0/4 for EFN#12; Figures 2E and 2F). Histological analysis revealed that the tumors consisted of small round blue cells that resembled Ewing sarcomas. However, tumor cells often showed osteoid formation (Figures 2G and S2B) and thus were considered small-cell osteosarcoma, which is a rare subtype of osteosarcomas. In addition, immunohistochemistry showed that the tumor cells expressed EWS-FLI1 and were frequently positive for Ki67, a marker for proliferating cells (Figure S2B).

Establishment of *EWS-FLI1*-Dependent Osteosarcoma Cell Lines

To further investigate the properties of the *EWS-FLI1*-induced osteosarcomas in detail, we established *EWS-FLI1*-dependent osteosarcoma cell lines from subcutaneous

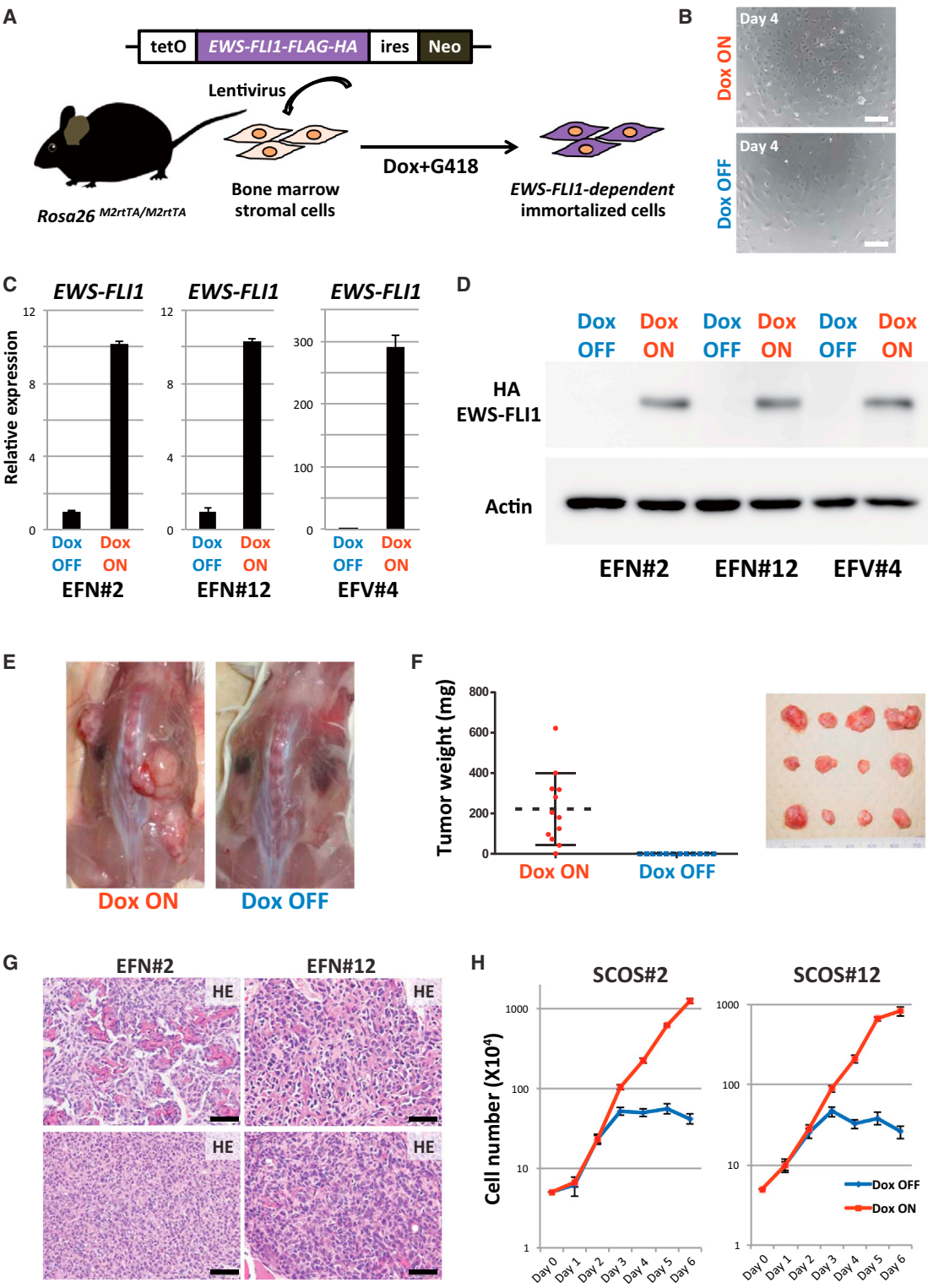

Figure 2. *EWS-FLI1*-Dependent Small-Cell Osteosarcoma Model by Utilizing the Lentiviral *EWS-FLI1* Expression System

(A) Schematic illustrations of the lentiviral *EWS-FLI1* expression system. Lentivirus was introduced into bone marrow stromal cells collected from *Rosa26-M2rtTA* mice. *EWS-FLI1*-expressing neomycin-resistant cells survived this protocol.

(legend continued on next page)

osteosarcomas in immunocompromised mice inoculated with EFN#2 and EFN#12 cells (SCOS#2 and SCOS#12, respectively). As observed in the primary *EWS-FLI1*-dependent immortalized cells, the established osteosarcoma cell lines expressed *EWS-FLI1* in a Dox concentration-dependent manner (Figure S2C) and actively proliferated in the presence of Dox (Figures 2H and S2D–S2F). After Dox withdrawal, SCOS#2 and SCOS#12 changed their morphology and stopped proliferating (Figure S2D). At the same time, we found increased expressions of p53 and p21, but no increase in β-gal (SAβgal) activity, which is associated with senescence (Figure S2G). Upon re-administration of Dox, the growth-arrested cells reacquired proliferative potential (Figure S2H). The reversible phenotype suggested that *EWS-FLI1* depletion results in cell-cycle arrest of the osteosarcoma cells.

Given that the genomic integration of lentivirus might play a role in osteosarcoma development, we also determined the virus integration site of SCOS#2. We identified a single integration at the intergenic region 13 kb downstream of *Cd14* (Figure S2I), a location unlikely to act as a genetic driver for sarcoma development.

To evaluate the similarity of the established *EWS-FLI1*-dependent sarcoma cell lines with human Ewing sarcomas and osteosarcomas, we compared global gene expression profiles of the SCOSs by microarray analysis. We first extracted genes that are specifically upregulated/downregulated in human Ewing sarcomas compared with human osteosarcomas and examined their expression in SCOS#2 and SCOS#12. We found that the gene expression patterns of SCOSs exhibit partial similarities with both human Ewing sarcomas and osteosarcomas (Figure S3A), suggesting that SCOSs have shared characteristics with both Ewing sarcomas and osteosarcomas.

Depletion of *EWS-FLI1* Expression Promoted Osteogenic Differentiation of Osteosarcoma Cells

To investigate the target of *EWS-FLI1*, we next compared gene expression profiles between *EWS-FLI1*-expressing and non-expressing sarcoma cells using SCOS#2 and SCOS#12. Intriguingly, in both cell lines, extracellular matrix and space-related genes, which often include bone and cartilage development-related genes, were significantly enriched in Dox OFF sarcoma cells (for 72 hr) compared with Dox ON *EWS-FLI1*-expressing sarcoma cells by GO enrichment analysis (Figures 3A, 3B, and S3B). Previous studies proposed that Ewing sarcoma could arise from mesenchymal stem cells (MSCs) (Riggi et al., 2008, 2014; Tirode et al., 2007). Long-term knockdown of *EWS-FLI1* with shRNA in Ewing sarcoma cells resulted in cellular differentiation to osteogenic, adipogenic, and chondrogenic lineage, consistent with an MSC origin of Ewing sarcoma (Tirode et al., 2007). Similarly, in the present study, the short-term depletion of *EWS-FLI1* in SCOS#2 and SCOS#12 resulted in the promotion of osteogenic differentiation with increased alkaline phosphatase activity (Figure 3C). Notably, after long-term depletion of *EWS-FLI1*, a subset of sarcoma cells slowly proliferated and exhibited heterogeneous morphology (Figure 3D). The *EWS-FLI1*-withdrawn sarcoma cells expressed higher levels of osteogenic differentiation marker genes, as well as chondrogenic and adipogenic genes (Figures 3E and S3C). Moreover, long-term culture without *EWS-FLI1* expression led to lipid production in a small subset of cells, as assessed by oil red O staining (Figure S3D).

SCOS#2 and SCOS#12 formed small-cell osteosarcomas in immunocompromised mice given Dox. These sarcoma cells had high proliferative activity based on Ki67 immunohistochemistry (Figure 3F). Consistent with in vitro findings that the growth of both SCOS#2 and SCOS#12 depends on *EWS-FLI1* expression, the subcutaneous tumors stopped or retarded their growth after the withdrawal of Dox in vivo (Figures 3F and 3G). Of particular note, histological analysis revealed that the Dox-withdrawn tumors consisted of osteoid and mature bone tissue with a small number of blue cells (Figure 3F). These results indicated that depletion of *EWS-FLI1* promoted osteogenic differentiation of

(B) The immortalized cells (EFN#2) grew rapidly in Dox-containing medium. Dox withdrawal resulted in growth retardation and morphological change in *EWS-FLI1*-expressing cells (4 days after the withdrawal). Scale bars, 200 μm.
(C) qRT-PCR results show *EWS-FLI1* mRNA expression in Dox-treated samples (24 hr). Data are presented as means ± SD (three technical replicates). The expression level of Dox OFF cells was set to 1.
(D) Western blotting using anti-HA antibody detected EWS-FLI1 protein in the presence of Dox (48 hr).
(E) *EWS-FLI1*-dependent immortalized cells (EFN#2) developed tumors in immunocompromised mice only in the presence of Dox (10 weeks after the transplantation).
(F) Tumor weight at 10 weeks after the transplantation of EFN#2 with/without Dox administration. Tumor development depended on Dox administration (n = 12, independent samples for each group). Error bars represent SD.
(G) Histology of *EWS-FLI1*-induced tumors in immunocompromised mice. Tumors are small-cell osteosarcomas, which consist of small blue round cells with various amounts of osteoid formation. The osteoid-rich region (upper) and small blue round cell-rich region (lower) are shown. Scale bars, 50 μm.
(H) Cell growth assay of the established *EWS-FLI1*-dependent sarcoma cell lines (SCOS#2 and SCOS#12). The growth of sarcoma cells depended on *EWS-FLI1* expression. Sarcoma cells without Dox exposure started to lose their growth at 3 days after Dox withdrawal. The means ± SD are shown in each group (two technical replicates per n; n = 3 biological replicates).

A

GO ACCESSION	GO Term	Corrected p-value
GO:0044421	extracellular region part	6.19E-18
GO:0005576	extracellular region	6.19E-18
GO:0031012	extracellular matrix	4.19E-10
GO:0005578	proteinaceous extracellular matrix	9.33E-09
GO:0005615	extracellular space	9.33E-09
GO:0005488	binding	1.37E-08
GO:0042127	regulation of cell proliferation	7.24E-08
GO:0008219	cell death	9.11E-07
GO:0016265	death	1.14E-06

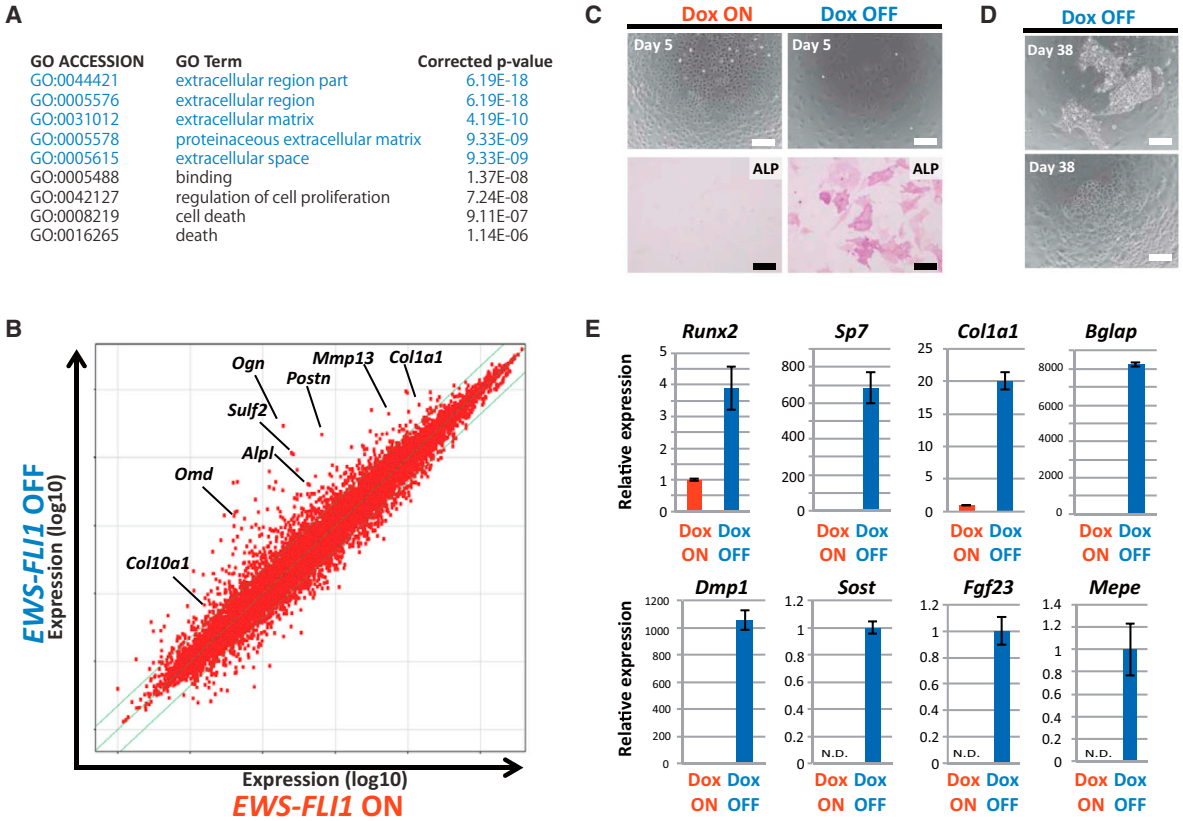

H

	Homer Known Motif	P-value	% of Targets	Best Match
1	ACTTTCGTTTCT	1E-35	2.42	T1ISRE
2	ATTTTCCATT	1E-22	20.17	NFATC1
3	ACGAGGAAGT	1E-22	12.76	ELF5(ETS)
4	ATTTCCTGTG	1E-18	13.58	EWS-ERG
5	GAGTTCCGGT	1E-18	13.58	Fli1
6	AACAGGAAAT	1E-17	8.58	EWS-FLI1

I

SK-N-MC (human Ewing sarcoma)

	De novo Motif	P-value	% of Targets	Best Match
1	ACGAAGGAAGGA	1E-1910	31.74	EWSR1-FLI1
2	AAGAAAGGAA	1E-600	35.04	EWSR1-FLI1
3	GAATGGAATGGA	1E-571	5.25	Zfp410
4	GATTTCCGGT	1E-435	18.29	ERG
5	TCTCGCGAGATC	1E-288	3.1	GFX

SCOS#2

	De novo Motif	P-value	% of Targets	Best Match
1	TAGTGGCTATCT	1E-182	12.60	Nkx2-6
2	ATTCTCGTCCTG	1E-171	18.18	AR-halfsite
3	TTGTGTCG	1E-171	16.97	Sox14
4	AAAAACAGGAAG	1E-157	12.02	Ets1
5	CTTGAAGAAA	1E-154	15.88	Tcfap2e

(legend on next page)

osteosarcoma cells in vivo. Together, our results highlight the role of *EWS-FLI1* expression on the suppression of terminal differentiation of osteosarcoma cells.

EWS-FLI1 Binds to the ETS Motif in *EWS-FLI1*-Induced Osteosarcoma Cells

To investigate how EWS-FLI1 suppresses the expression of osteogenic differentiation-related genes, we performed chromatin immunoprecipitation sequencing (ChIP-seq) analysis for hemagglutinin (HA)-tagged EWS-FLI1 in SCOS#2 cells using anti-HA antibody. The analysis identified 2,562 sites for EWS-FLI1 binding in *EWS-FLI1*-expressing SCOS#2. A motif analysis with HOMER (hypergeometric optimization of motif enrichment) revealed that these binding sites often contain the ETS binding motif (Figure 3H), suggesting that EWS-FLI1 binds to the genome through the C-terminal ETS binding domain of FLI1. Previous studies demonstrated that EWS-FLI1 binds DNA preferentially at GGAA repeats to activate transcription. Indeed, we confirmed that the GGAA repeat is the most representative motif of EWS-FLI1 binding in SK-N-MC, a human Ewing sarcoma cell line (Figure 3I) (Riggi et al., 2014). Notably, the GGAA repeat was not enriched in SCOS#2 according to de novo motif analysis for EWS-FLI1 binding (Figure 3I).

One target of EWS-FLI1 in human Ewing sarcoma, *Nr0b1*, has 15 GGAA repeats 50 kb upstream from its transcription start site (TSS) in mouse. ChIP-seq data revealed that EWS-FLI1 does not bind to these GGAA repeats in SCOS#2, which is consistent with the fact that *Nr0b1* expression is not affected by EWS-FLI1 expression in SCOS#2 (data not shown). We found similar GGAA repeats upstream and downstream of *Nkx2-2*, *Ccnd1*, and *Dkk2*, which are also known targets of EWS-FLI1 binding in human Ewing sarcomas. However, there was no clear enrichment of EWS-FLI1 binding in SCOS#2. Ultimately, we found that only four of 2,562 EWS-FLI1 binding sites in SCOS#2 contained more than ten GGAA repeats, highlighting the difference in EWS-FLI1 binding between human Ewing sarcomas and our *EWS-FLI1*-induced osteosarcoma cells.

To further assess whether EWS-FLI1 binding affects the expression of adjacent genes, we first identified 126 genes that possess EWS-FLI1 binding sites close to their TSS (±5 kb) and compared the expression between Dox (*EWS-FLI1*) ON and Dox OFF cells. No obvious difference in the expression levels of these genes was detected (Figure S4A). Similarly, EWS-FLI1 binding was not enriched near the TSSs of the genes upregulated or downregulated by Dox exposure (517 and 588 genes, respectively; cutoff point at fold change >1.5; Figure S4B). In contrast, the genome-wide analysis of EWS-FLI1 binding revealed that EWS-FLI1 was preferentially recruited to the distal intergenic region (72.5% of total binding sites) (Figures S4C and S4D). Our results indicate that EWS-FLI1 binds to the genome via the ETS motif, but EWS-FLI1 binding at the proximal regulatory region does not have a substantial impact on altered gene expressions in *EWS-FLI1*-induced osteosarcoma cells.

Establishment of iPSCs from *EWS-FLI1*-Induced Osteosarcoma Cells

The derivation of iPSCs does not require specific changes in the genomic sequence, making this technology applicable for the evaluation of genetic context effects on cell types and differentiation statuses. Given that additional genetic aberrations may be required for *EWS-FLI1*-induced sarcoma development, the establishment of iPSCs from *EWS-FLI1*-induced sarcoma cells should provide a unique

Figure 3. Inhibition of Osteogenic Differentiation by *EWS-FLI1* in Small-Cell Osteosarcoma Cells

(A) Gene ontology enrichment analysis showed that the extracellular region and matrix-related genes are upregulated 72 hr after Dox withdrawal in SCOS#2 cells. The upregulated genes were selected by cutoff point at hold change >1.5 and $p < 1.0 \times 10^{-4}$. The top five enriched clusters are highlighted.

(B) Scatterplot analysis revealed that a number of osteogenesis and chondrogenesis-related genes were upregulated 72 hr after Dox withdrawal in SCOS#2 cells.

(C) At 5 days after Dox withdrawal, sarcoma cells exhibited alkaline phosphatase activity. Scale bars, 50 μm (upper) and 200 μm (lower).

(D) At 38 days after Dox withdrawal, slow-growing heterogeneous cells were observed. Scale bars, 200 μm.

(E) At 38 days after Dox withdrawal, cells showed higher expression of osteogenic differentiation-related genes. mRNA expression levels were measured by qRT-PCR. Data are presented as means ± SD (three technical replicates). The expression level of Dox ON cells was set to 1. *Sost*, *Fgf23*, and *Mepe* were undetectable in Dox ON samples by qRT-PCR, therefore, the expression level of Dox OFF cells was set to 1 instead.

(F) H&E and alizarin red staining demonstrated that Dox withdrawal leads to a significant reduction of the small blue cell population and an increase of mature bone formation. Ki67 immunohistochemistry shows the active proliferation of sarcoma cells in Dox ON condition. Scale bars, 200 μm (upper) and 50 μm (lower).

(G) In vivo tumor formation assay using sarcoma cell line SCOS#2 (n = 7, independent tumor). Dox treatment was withdrawn at 3 weeks, and mice were sacrificed at 7 weeks.

(H) The ETS motif was enriched in EWS-FLI1 binding sites according to motif analysis with HOMER of SCOS#2.

(I) De novo motif analysis identified the GGAA repeat as the most frequent motif in SK-N-MC. This repeat was not found in SCOS#2.

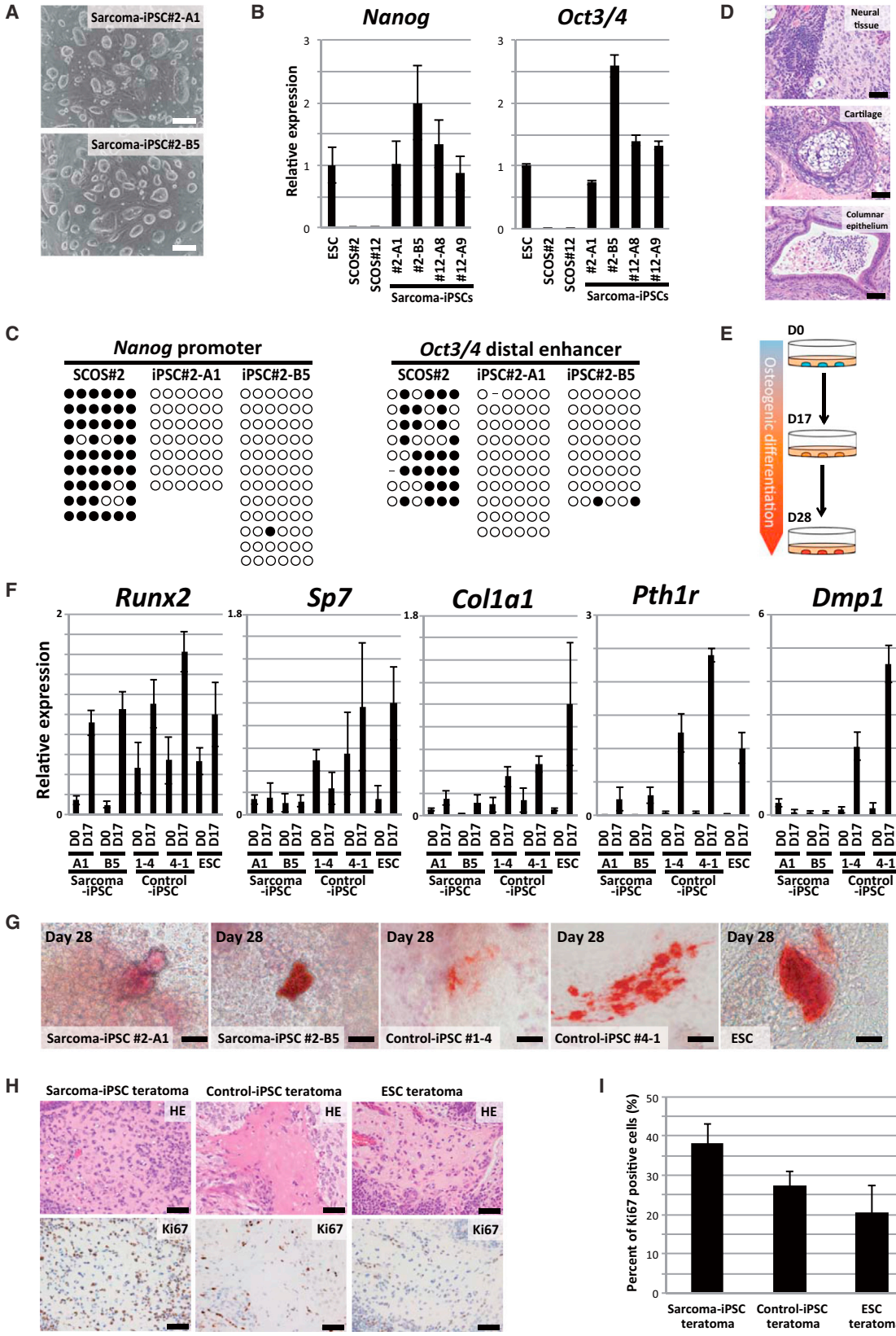

(legend on next page)

tool to study the impact of genetic abnormalities beyond *EWS-FLI1* expression on sarcoma development. We therefore tried to establish iPSCs from SCOS#2 and SCOS#12. After single-cell cloning of sarcoma cells, we introduced *OCT3/4, SOX2, KLF4*, and *c-MYC* into the sarcoma cells and obtained iPSC-like colonies under the absence of *EWS-FLI1* expression (efficiency of colony formation was 0.0009%; Figures 4A and S5A). These iPSC-like cells expressed pluripotency-related genes, such as *Nanog* and *Oct3/4*, at comparative levels with ESCs (Figure 4B). Similarly, the global gene expression patterns of iPSC-like cells were similar to those in normal ESCs and control iPSCs (Figure S5B).

The sarcoma-derived iPSC-like cells exhibited demethylation of both *Nanog* promoter and *Oct3/4* distal enhancer (Figure 4C), implying that these cells underwent epigenetic reorganization to acquire pluripotency. The silencing of the four exogenous factors, which occurs in the late stage of cellular reprogramming, was observed in some iPSC-like clones (Figure S5C), suggesting that these cells were fully reprogrammed. Then, we performed array comparative genomic hybridization (array CGH) and found that the single-cell-derived sarcoma cells had extensive chromosomal abnormalities (Figure S5D). Notably, sarcoma-derived iPSC-like cells harbored some identical chromosomal aberrations (Figure S5D). Furthermore, exome analysis revealed hundreds of identical missense mutations between SCOS#2 and sarcoma-derived iPSC-like cells (Figure S5E and Table S2), affirming that these iPSC-like clones were derived from the parental sarcoma cell. A subset of the mutated genes was also mutated in human Ewing sarcomas and osteosarcomas by the COSMIC database (http://cancer.sanger.ac.uk/cosmic) (Table S3). These sarcoma-derived iPSC-like cells lacked the ability to contribute to adult chimeric mice by blastocyst injection (data not shown), presumably because of the extensive genetic abnormalities observed in the CGH analysis and exome analysis. However, sarcoma-derived iPSC-like cells formed teratomas consisting of cells differentiating into three different germ layers when they were inoculated into the subcutaneous tissue of immunocompromised mice (Figure 4D), indicating that they have pluripotency. These results affirm that we succeeded in generating iPSCs from *EWS-FLI1*-induced osteosarcoma cells.

Sarcoma iPSCs Exhibit Impaired Osteogenic Differentiation Irrespective of *EWS-FLI1* Expression

The enhanced osteogenic differentiation of sarcoma cells upon the depletion of *EWS-FLI1* raised the possibility that *EWS-FLI1*-dependent osteosarcomas arise from osteogenic cells. Accordingly, we tried to induce osteogenic cells, a putative cell of origin of the sarcomas, from pluripotent stem cells in vitro in the absence of *EWS-FLI1* expression (Figure 4E) (Kim et al., 2010). In control ESCs and control iPSCs established from the fibroblasts of *EWS-FLI1*-inducible chimeric mice (*Rosa-M2rtTA/Rosa:tetO-EWS-FLI1*), osteogenic differentiation stimuli induced osteogenic differentiation-related genes, such as *Runx2, Sp7, Col1a1, Pth1r*, and *Dmp1* (day 17) (Figure 4F). Although the stimuli also induced the expression of *Runx2*, a key transcription factor for osteogenic

Figure 4. Establishment of Sarcoma-Derived iPSCs and Differentiation of Sarcoma iPSCs into Osteogenic Cells

(A) iPSCs-like cells were established from sarcoma cells by introducing reprogramming transcription factors. Scale bars, 200 μm.

(B) qRT-PCR revealed that the expression levels of pluripotency-related genes in sarcoma-derived iPSC-like cells were equivalent to those of ESCs. Data are presented as means ± SD (three technical replicates). The expression level of ESCs was set to 1.

(C) Bisulfite sequencing analyses revealed that the *Nanog* promoter and the *Oct3/4* distal enhancer region are demethylated in sarcoma-derived iPSC-like cells. White and black circles indicate non-methylated and methylated cytosine at CpG sites, respectively.

(D) Sarcoma iPSCs gave rise to teratomas consisting of ectodermal, mesodermal, and endodermal tissue in the subcutaneous tissue of immunocompromised mice. Scale bars, 50 μm.

(E) Schematic illustrations of in vitro osteogenic differentiation.

(F) qRT-PCR analysis of osteogenic differentiation-related genes. Wild-type ESCs (V6.5), *EWS-FLI1*-inducible ESCs (*Rosa-M2rtTA/Rosa::tetO-EWS-FLI1*), and two independent fibroblast-derived iPSCs with *Rosa-M2rtTA/Rosa::tetO-EWS-FLI1* alleles were used as controls in the osteogenic differentiation experiments. Sarcoma-derived iPSCs and control ESCs/iPSCs on day 0 and day 17 during osteogenic differentiation were examined for the expression of osteogenic differentiation-related genes. The mean ± SD is shown (three technical replicates per n; n = 3 biological replicates). The mean expression level of ESCs on day 17 was set to 1.

(G) Alizarin red staining revealed extracellular calcium deposits stained in blight reddish orange (day 28 after the induction of osteogenic differentiation). Scale bars, 20 μm.

(H) Histological analysis of an osteogenic region with osteoid production in teratomas. Ki67 immunohistochemistry revealed that osteoid-producing cells derived from sarcoma iPSCs have higher proliferative activities than those derived from control ESCs/iPSCs. Scale bars, 50 μm.

(I) Ki67 positive ratio of osteogenic regions in teratomas derived from sarcoma iPSCs or control ESCs/iPSCs. The mean ± SD of six independent osteogenic regions in two independent sarcoma iPSCs teratomas, five independent osteogenic regions in the control iPSC teratomas, and nine independent osteogenic regions in two independent ESC teratomas are shown. The ANOVA test was used for the statistical analysis. Sarcoma iPSCs vs control iPSCs, $p < 0.05$; sarcoma iPSCs vs control ESCs, $p < 0.01$; control ESCs vs control iPSCs, $p > 0.05$.

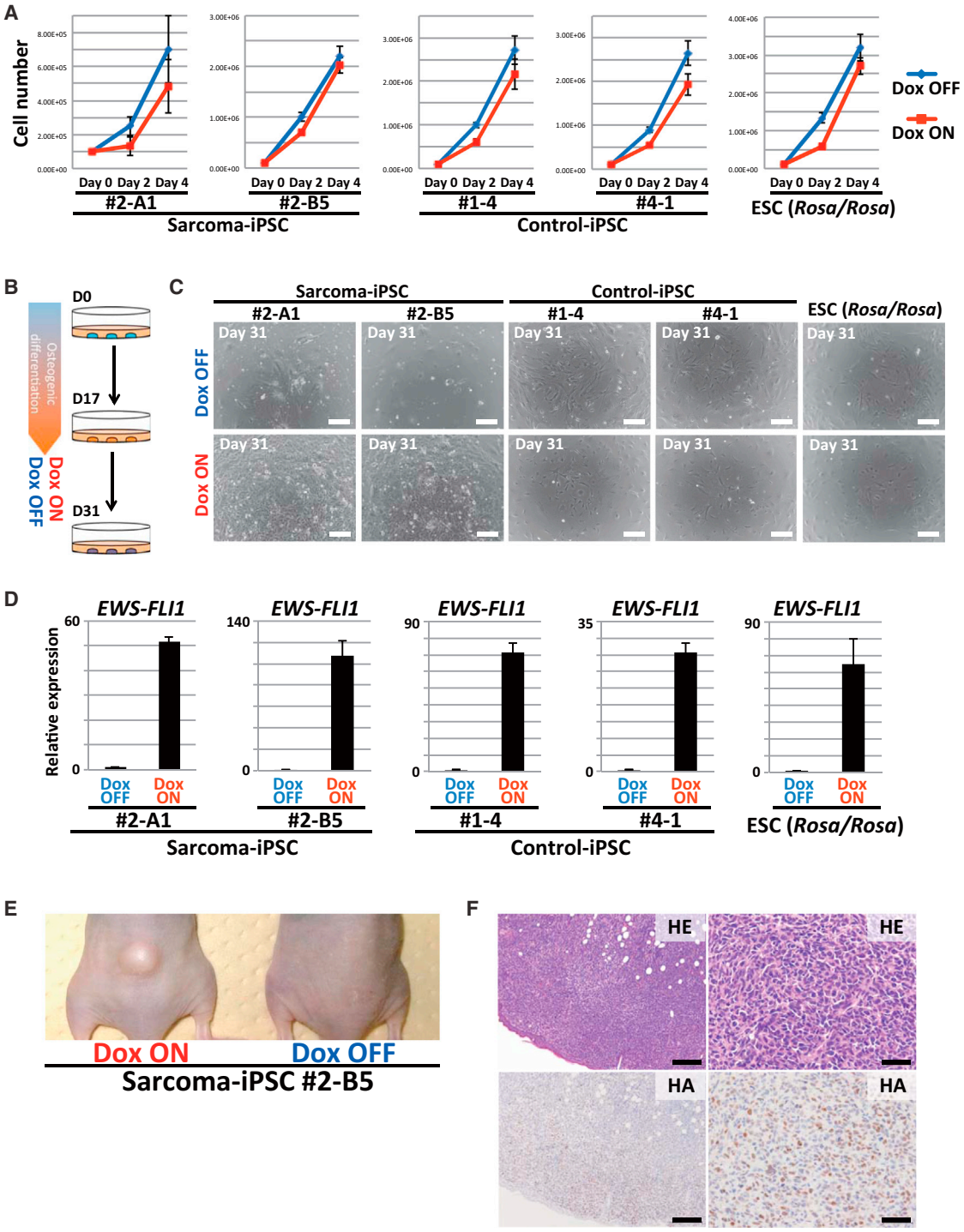

Figure 5. *EWS-FLI1* Induces Sarcomas from Induced Osteogenic Cells in Concert with Genetic Aberrations

(A) *EWS-FLI1* expression does not promote the growth of undifferentiated pluripotent stem cells. The means ± SD are shown in each group (two technical replicates per n; n = 3 biological replicates).

(B) Schematic illustration of in vitro osteogenic differentiation and *EWS-FLI1* induction. The induced osteogenic cells (17 days after the induction of osteogenic differentiation) were subsequently treated with/without Dox for 2 weeks.

(C) The sarcoma iPSC-derived osteogenic cells acquired robust proliferation with Dox treatment, whereas control ESCs/iPSCs (*Rosa-M2rtTA/Rosa*::*tetO-EWS-FLI1*)-derived osteogenic cells did not. Scale bars, 200 μm.

(legend continued on next page)

differentiation, in sarcoma-derived iPSCs, the induction of osteogenic genes downstream of *Runx2* was impaired even in the absence of *EWS-FLI1* expression (day 17) (Figure 4F). Upon the prolonged induction of osteogenic differentiation (day 28), a mineralized region, as assessed by alizarin red staining, was detected in all samples (Figure 4G). However, the mineralized area was larger in control ESCs/iPSCs than in sarcoma-derived iPSCs (Figure 4G). We also employed the in vivo differentiation method of sarcoma iPSCs to generate teratomas in immunocompromised mice. Both the sarcoma iPSCs and the control ESCs/iPSCs formed teratomas, which contained an osteogenic region in the absence of *EWS-FLI1* expression (Figure 4H). The Ki67-positive ratio of sarcoma iPSC-derived osteogenic cells was significantly higher than that of control ESC/iPSC-derived osteogenic cells ($p < 0.05$ and $p < 0.01$, respectively) (Figure 4I). Collectively, sarcoma-derived iPSCs exhibit impaired osteogenic differentiation irrespective of *EWS-FLI1* expression, suggesting that genetic and epigenetic alterations besides *EWS-FLI1* fusion also inhibit osteogenic differentiation and maintain the proliferating progenitor state.

EWS-FLI1 Expression Induced Rapid Sarcoma Development from Sarcoma iPSC-Derived Osteogenic Cells

Finally, we tried to analyze the cooperative action between *EWS-FLI1* expression and the impaired differentiation associated with genetic aberrations on sarcoma development. *EWS-FLI1* expression in both sarcoma iPSCs and control ESCs/iPSCs (*Rosa-M2rtTA/Rosa*::*tetO-EWS-FLI1*) has no promoting effect on cell growth under undifferentiated culture conditions (Figure 5A). Next, we induced osteogenic differentiation of sarcoma iPSCs and control cells in vitro and then *EWS-FLI1* expression (Figure 5B). At day 17 of the osteogenic differentiation protocol, osteogenic precursor cells derived from sarcoma iPSCs and control cells were treated with Dox (Figure 5B). Of note, only the sarcoma-derived osteogenic cells showed robust proliferation in vitro in response to Dox at day 31 (Figures 5C and 5D). Xenograft of these cells resulted in tumor development only in mice given Dox (Figure 5E). Histological analysis revealed that these xenograft tumors were sarcomas that consisted of small round blue cells (Figure 5F). The secondary sarcoma harbored shared genetic mutations with SCOS (Figure S5E and Table S2). Osteogenic cells derived from control ESCs/iPSCs did not exhibit obvious *EWS-FLI1*-dependent growth in vivo (data not shown), affirming that sarcoma development requires additional aberrations. Interestingly, these tumors often contained a carcinoma component, therefore they were regarded as carcinosarcomas (Figure S5F). Presumably, this component reflected the contamination of heterogeneous cell types after in vitro osteogenic differentiation of the sarcoma iPSCs. Together, these results suggest that the impaired differentiation potential associated with the sarcoma genome contributes to a rapid malignant transformation of osteogenic cells upon *EWS-FLI1* expression.

DISCUSSION

Although the exact cell of origin of Ewing sarcoma remains to be determined, it is suggested that Ewing sarcomas may arise from MSCs, which reside in the bone marrow (Riggi et al., 2008; Tirode et al., 2007). In the present study, we introduced the *EWS-FLI1* fusion gene to bone marrow stromal cells to establish an Ewing sarcoma mouse model (Castillero-Trejo et al., 2005; Riggi et al., 2005). We successfully generated *EWS-FLI1*-induced sarcomas that depended on *EWS-FLI1* expression in terms of in vitro proliferation and in vivo tumor development. However, the developed tumors were small-cell osteosarcomas composed of small round blue cells with osteoid formation. Small-cell osteosarcoma is a rare subtype of osteosarcomas, accounting for 1%–1.5% of all osteosarcomas (Nakajima et al., 1997). Notably, small-cell osteosarcoma exhibits shared properties with Ewing sarcoma (Righi et al., 2015). Moreover, *EWSR1* rearrangement, which includes *EWS-FLI1*, has been identified in a subset of small-cell osteosarcomas (Dragoescu et al., 2013; Hill et al., 2002; Noguera et al., 1990; Oshima et al., 2004). The results of the present study demonstrate that the *EWS-FLI1* fusion gene could function as a driver oncogene in a particular type of osteosarcoma and suggest that our model could be a rodent model for *EWS-FLI1*-dependent osteosarcomas.

The inhibition of differentiation has been considered to play a role in many types of tumor development through maintenance of the proliferating progenitor cell state. Previous studies demonstrated that the knockdown of *EWS-FLI1* in Ewing sarcoma cell lines results in osteogenic, adipogenic and chondrogenic differentiation (Tirode et al., 2007). Similarly, in the present study, we found that

(D) *EWS-FLI1* expression in the induced osteogenic cells was detectable by Dox exposure in qRT-PCR analyses. Data are presented as means ± SD (three technical replicates). The mean expression level of Dox OFF was set to 1.
(E) Osteogenic cells induced with *EWS-FLI1* developed tumors in immunocompromised mice only in the presence of Dox (after 3–7 weeks of treatment).
(F) Histologically, developed tumors were sarcomas consisting of small round blue cells that resembled small-cell osteosarcomas. HA immunohistochemistry revealed that sarcoma cells express EWS-FLI1. Scale bars, 200 μm (left) and 50 μm (right).

EWS-FLI1-induced osteosarcomas exhibit robust osteogenic differentiation after the withdrawal of *EWS-FLI1* expression, indicating that *EWS-FLI1* expression inhibits osteogenic differentiation. Molecular mechanisms by which *EWS-FLI1* expression blocks osteogenic differentiation have been proposed in previous studies. It was reported that EWS-FLI1 inhibits osteogenic differentiation in murine multipotent mesenchymal cells by binding to Runx2, an osteogenic transcription factor, and inhibiting its function (Li et al., 2010). Similarly, EWSR1 was shown to interact with SOX9, which is involved in chondrogenic differentiation in zebrafish (Merkes et al., 2015). However, we failed to detect a physical interaction between EWS-FLI1 and Runx2 or Sox9 in our osteosarcoma cells by immunoprecipitation (data not shown), suggesting that another mechanism may exist for the defective differentiation. Notably, Riggi et al. (2014) demonstrated that EWS-FLI1 expression causes the displacement of endogenous ETS transcription factors and p300 at the canonical ETS motifs in Ewing sarcoma cells. We found that EWS-FLI1 binds to the genome through the ETS motif in *EWS-FLI1*-dependent osteosarcoma cells. Given that the ETS family of transcription factors plays an important role in osteogenic differentiation as well as adipogenic and chondrogenic differentiation (Birsoy et al., 2011; Iwamoto et al., 2007; Raouf and Seth, 2000), the aberrantly occupied ETS motifs by EWS-FLI1 might inhibit ETS family-mediated differentiation, resulting in maintenance of the proliferating progenitor state.

The majority of Ewing sarcomas arise in adolescence. Considering the young age at onset, it is suggested that Ewing sarcoma harbors few genetic abnormalities besides the *EWS-FLI1* fusion gene. Indeed, recent genome-wide sequencing analyses revealed a paucity of somatic abnormalities (Crompton et al., 2014; Tirode et al., 2014). However, consistent with a number of previous studies, we failed to induce sarcomas by the sole expression of *EWS-FLI1* in a variety of cell types in vivo, providing additional evidence that *EWS-FLI1* expression is not sufficient for sarcoma development. Thus, we established iPSCs from *EWS-FLI1*-induced osteosarcoma cells, thereby harboring the same genetic abnormalities as the parental osteosarcoma cells. Interestingly, upon the induction of osteogenic differentiation, *EWS-FLI1* expression turned sarcoma iPSC-derived osteogenic cells into sarcoma cells, whereas the expression was not sufficient for the transformation of those from control ESCs/iPSCs.

It is noteworthy that sarcoma iPSCs showed an impairment of terminal osteogenic differentiation ability irrespective of *EWS-FLI1* expression. Notably, we found that osteogenic lineage cells derived from sarcoma iPSCs exhibit higher proliferating activity compared with cells derived from control ESCs/iPSCs. Taken together, it is conceivable that the additive effect by both *EWS-FLI1* expression and the defective differentiation properties of sarcoma iPSCs promotes sarcoma development by suppressing terminal differentiation and maintaining the proliferating progenitor state.

The causative aberration of the impaired differentiation properties of sarcoma iPSCs remains unclear. Recently, Lee et al. (2015) established iPSCs from patients with Li-Fraumeni syndrome and demonstrated that mutant p53 causes defective osteoblastic differentiation. However, we failed to detect the *Trp53* mutation in our sarcoma-derived iPSCs (Table S2), implying an alternative mechanism impairs osteogenic differentiation. Intriguingly, we observed that sarcoma iPSC teratomas sometimes exhibited impaired terminal differentiation of other lineages, which is also consistent with the fact that they lack the potential to make chimeric mice (Figure S5G). It is likely that a summation of extensive genetic abnormalities and epigenetic alterations is associated with the impaired differentiation of sarcoma iPSCs into multiple lineages. Further analysis is needed to determine the aberrations required for the sarcoma development associated with *EWS-FLI1* expression.

The fact that the in vitro induction of osteogenic differentiation leads to sarcoma development from sarcoma iPSCs in concert with *EWS-FLI1* expression indicates that these sarcomas arise from osteogenic progenitor cells. However, it is important to note that the withdrawal of *EWS-FLI1* in osteosarcoma cells resulted in increased expression of multiple genes involved in chondrogenic and adipogenic differentiation in addition to osteogenic differentiation-related genes. Together with previous findings on Ewing sarcoma, multipotent progenitors that have partial commitment to the osteogenic lineage in the bone marrow could be a cell of origin for *EWS-FLI1*-induced osteosarcomas. This notion is also supported by the fact that a subset of small-cell osteosarcomas exhibits both chondrogenic and osteogenic differentiation (Dragoescu et al., 2013; Nakajima et al., 1997).

In summary, we established an *EWS-FLI1*-dependent small-cell osteosarcoma model by introducing *EWS-FLI1* in mouse bone marrow stromal cells. We revealed that the impaired differentiation associated with both *EWS-FLI1* expression and sarcoma-associated genetic abnormalities plays a critical role in the development and maintenance of *EWS-FLI1*-induced osteosarcomas. We propose that targeting impaired terminal differentiation could be a possible therapeutic strategy for *EWS-FLI1*-induced sarcomas.

EXPERIMENTAL PROCEDURES

In Vivo Experiment

Rosa-M2rtTA/Rosa:tetO-EWS-FLI1 and *Rosa-M2rtTA/Col1a1::tetO-EWS-FLI1* chimeric mice were generated with KH2 (Beard et al., 2006). *Rosa-M2rtTA/Rosa::tetO-EWS-FLI1* mice and immunocompromised mice inoculated with sarcoma cells were treated with

Dox-containing water at 2 mg/ml with 10 mg/ml sucrose. *Rosa-M2rtTA/Col1a1::tetO-EWS-FLI1* mice were treated with lower concentrations of Dox (100 μg/ml to 2 mg/ml) because of early lethality. For the xenograft assay, a total of 3×10^6 *EWS-FLI1*-dependent immortalized cells, *EWS-FLI1*-dependent sarcoma cells, or ESCs/iPSCs were transplanted to immunocompromised mice. All animal experiments were approved by the CiRA Animal Experiment Committee, and the care of the animals was in accordance with institutional guidelines.

iPSC Induction and Maintenance

iPSC induction was performed by utilizing retroviral vectors (pMX-hOCT3/4, pMX-hSOX2, pMX-hKLF4, and pMX-hc-MYC; Addgene). Reprogramming factor-inducing single-cell-derived sarcoma cells were cultured in ESC media supplemented with human recombinant leukemia inhibitory factor (LIF; Wako), 2-mercaptoethanol (Invitrogen), and 50 μg/ml L-ascorbic acid (Sigma), and the established iPSCs were maintained with ESC media supplemented with LIF, 1 μM PD0325901 (Stemgent), and 3 μM CHIR99021 (Stemgent).

In Vitro Differentiation of ESC/iPSCs to Osteogenic Lineage

We employed the in vitro osteogenic differentiation protocol as described by Kim et al. (2010) with slight modifications. Briefly, 5,000 ESCs or iPSCs were cultured in a 96-well plate (Nunclon Sphere, Thermo Scientific) with ES differentiation media (Iscove's modified Dulbecco's medium, 15% FBS, penicillin/streptomycin, L-glutamine, L-ascorbic acid, transferrin, thioglycerol) for 2 days. On day 2, retinoic acid was added (final concentration, 10^{-6} M). On day 5, embryoid bodies were collected, transferred to a 6-well tissue culture dish, and cultured in osteogenic differentiation media (α minimal essential medium, 10% FBS, penicillin/streptomycin, L-glutamine, 2 nM triiodothyronine, ITS). The media were changed every other day. On day 17, RNA was extracted, and osteogenic gene expression of the induced osteogenic cells was confirmed by real-time quantitative RT-PCR. Alizarin red staining was performed on day 28.

Array Comparative Genomic Hybridization

Genomic DNA was extracted with PureLink Genomic DNA Mini Kit (Invitrogen). Array comparative genomic hybridization analysis was performed with SurePrint G3 Mouse Genome CGH Microarray Kit (Agilent) and analyzed with Agilent Genomic Workbench 7.0.

Microarray Analysis

200 ng of total RNA prepared with an RNeasy Mini Kit was subjected to cDNA synthesis with a WT Expression Kit (Ambion), and the resultant cDNA was fragmented and hybridized to a Mouse Gene 1.0 ST Array (Affymetrix). The data obtained were analyzed using GeneSpring GX software (version 13.0, Agilent Technologies).

ChIP-Seq Analysis

ChIP (formaldehyde-assisted isolation of regulatory elements) was performed as described previously (Arioka et al., 2012). Anti-HA antibody (Nacalai, HA124, 06340-54) was used for the ChIP-seq analysis. Sequencing libraries were generated using a TruSeq ChIP Sample Prep Kit (Illumina). The libraries were sequenced to generate single-end 100-bp reads using Illumina MiSeq. We used the MACS (Zhang et al., 2008) version 1.4.2 peak finding algorithm to identify regions of ChIP-seq enrichment over background with a p value 1×10^{-3}. Ngs.plot was used to analyze and visualize the mapped reads (Shen et al., 2014). The motif analysis was performed using HOMER software (Heinz et al., 2010).

Exome Analysis

Genomic DNA of SCOS#2-A1, sarcoma iPSC#2-A1, and sarcoma-iPSC#2-A1-derived secondary sarcoma was extracted with a PureLink Genomic DNA Mini Kit (Invitrogen). Whole-exome capture was done with SureSelect XT (Agilent Technologies). The exome libraries were then sequenced on a HiSeq2500 (Illumina).

ACCESSION NUMBERS

The accession number for the data reported in this article is GEO: GSE72898.

SUPPLEMENTAL INFORMATION

Supplemental Information includes Supplemental Experimental Procedures, five figures, and four tables and can be found with this article online at http://dx.doi.org/10.1016/j.stemcr.2016.02.009.

AUTHOR CONTRIBUTIONS

S.K. and Y.Y. proposed the research project, designed the experiments, performed the experiments, and wrote the manuscript. T.Y., S.K., K.S., and F.I. analyzed microarray, ChIP-seq, and exome sequencing data. A.H., K.W., T.O., H.A., and K.S. provided technical instruction. K.S., H.S., and T.Y. analyzed data.

ACKNOWLEDGMENTS

We are grateful to P. Karagiannis for critical reading of this manuscript, and T. Ukai, M. Yagi, T. Sato, and K. Osugi for technical assistance. The authors were supported in part by P-DIRECT, a Grant-in-Aid from the Ministry of Education, Culture, Sports, Science, and Technology of Japan, the Ministry of Health, Labor, and Welfare of Japan, SICORP, the Takeda Science Foundation, and the Naito Foundation.

Received: September 18, 2015
Revised: February 15, 2016
Accepted: February 16, 2016
Published: March 17, 2016

REFERENCES

Arioka, Y., Watanabe, A., Saito, K., and Yamada, Y. (2012). Activation-induced cytidine deaminase alters the subcellular localization of Tet family proteins. PLoS One *7*, e45031.

Beard, C., Hochedlinger, K., Plath, K., Wutz, A., and Jaenisch, R. (2006). Efficient method to generate single-copy transgenic mice

by site-specific integration in embryonic stem cells. Genesis *44*, 23–28.

Birsoy, K., Berry, R., Wang, T., Ceyhan, O., Tavazoie, S., Friedman, J.M., and Rodeheffer, M.S. (2011). Analysis of gene networks in white adipose tissue development reveals a role for ETS2 in adipogenesis. Development *138*, 4709–4719.

Castillero-Trejo, Y., Eliazer, S., Xiang, L., Richardson, J.A., and Ilaria, R.L., Jr. (2005). Expression of the EWS/FLI-1 oncogene in murine primary bone-derived cells results in EWS/FLI-1-dependent, Ewing sarcoma-like tumors. Cancer Res. *65*, 8698–8705.

Crompton, B.D., Stewart, C., Taylor-Weiner, A., Alexe, G., Kurek, K.C., Calicchio, M.L., Kiezun, A., Carter, S.L., Shukla, S.A., Mehta, S.S., et al. (2014). The genomic landscape of pediatric Ewing sarcoma. Cancer Discov. *4*, 1326–1341.

Dragoescu, E., Jackson-Cook, C., Domson, G., Massey, D., and Foster, W.C. (2013). Small cell osteosarcoma with Ewing sarcoma breakpoint region 1 gene rearrangement detected by interphase fluorescence in situ hybridization. Ann. Diagn. Pathol. *17*, 377–382.

Grunewald, T.G., Bernard, V., Gilardi-Hebenstreit, P., Raynal, V., Surdez, D., Aynaud, M.M., Mirabeau, O., Cidre-Aranaz, F., Tirode, F., Zaidi, S., et al. (2015). Chimeric EWSR1-FLI1 regulates the Ewing sarcoma susceptibility gene EGR2 via a GGAA microsatellite. Nat. Genet. *47*, 1073–1078.

He, B.C., Chen, L., Zuo, G.W., Zhang, W., Bi, Y., Huang, J., Wang, Y., Jiang, W., Luo, Q., Shi, Q., et al. (2010). Synergistic antitumor effect of the activated PPARgamma and retinoid receptors on human osteosarcoma. Clin. Cancer Res. *16*, 2235–2245.

Heinz, S., Benner, C., Spann, N., Bertolino, E., Lin, Y.C., Laslo, P., Cheng, J.X., Murre, C., Singh, H., and Glass, C.K. (2010). Simple combinations of lineage-determining transcription factors prime cis-regulatory elements required for macrophage and B cell identities. Mol. Cell *38*, 576–589.

Hill, D.A., O'Sullivan, M.J., Zhu, X., Vollmer, R.T., Humphrey, P.A., Dehner, L.P., and Pfeifer, J.D. (2002). Practical application of molecular genetic testing as an aid to the surgical pathologic diagnosis of sarcomas: a prospective study. Am. J. Surg. Pathol. *26*, 965–977.

Iwamoto, M., Tamamura, Y., Koyama, E., Komori, T., Takeshita, N., Williams, J.A., Nakamura, T., Enomoto-Iwamoto, M., and Pacifici, M. (2007). Transcription factor ERG and joint and articular cartilage formation during mouse limb and spine skeletogenesis. Dev. Biol. *305*, 40–51.

Kim, K., Doi, A., Wen, B., Ng, K., Zhao, R., Cahan, P., Kim, J., Aryee, M.J., Ji, H., Ehrlich, L.I., et al. (2010). Epigenetic memory in induced pluripotent stem cells. Nature *467*, 285–290.

Kinsey, M., Smith, R., and Lessnick, S.L. (2006). NR0B1 is required for the oncogenic phenotype mediated by EWS/FLI in Ewing's sarcoma. Mol. Cancer Res. *4*, 851–859.

Lee, D.F., Su, J., Kim, H.S., Chang, B., Papatsenko, D., Zhao, R., Yuan, Y., Gingold, J., Xia, W., Darr, H., et al. (2015). Modeling familial cancer with induced pluripotent stem cells. Cell *161*, 240–254.

Li, X., McGee-Lawrence, M.E., Decker, M., and Westendorf, J.J. (2010). The Ewing's sarcoma fusion protein, EWS-FLI, binds Runx2 and blocks osteoblast differentiation. J. Cell Biochem. *111*, 933–943.

Lin, P.P., Pandey, M.K., Jin, F., Xiong, S., Deavers, M., Parant, J.M., and Lozano, G. (2008). EWS-FLI1 induces developmental abnormalities and accelerates sarcoma formation in a transgenic mouse model. Cancer Res. *68*, 8968–8975.

Luo, X., Chen, J., Song, W.X., Tang, N., Luo, J., Deng, Z.L., Sharff, K.A., He, G., Bi, Y., He, B.C., et al. (2008). Osteogenic BMPs promote tumor growth of human osteosarcomas that harbor differentiation defects. Lab Invest. *88*, 1264–1277.

Merkes, C., Turkalo, T.K., Wilder, N., Park, H., Wenger, L.W., Lewin, S.J., and Azuma, M. (2015). Ewing sarcoma ewsa protein regulates chondrogenesis of Meckel's cartilage through modulation of Sox9 in zebrafish. PLoS One *10*, e0116627.

Miyagawa, Y., Okita, H., Nakaijima, H., Horiuchi, Y., Sato, B., Taguchi, T., Toyoda, M., Katagiri, Y.U., Fujimoto, J., Hata, J., et al. (2008). Inducible expression of chimeric EWS/ETS proteins confers Ewing's family tumor-like phenotypes to human mesenchymal progenitor cells. Mol. Cell Biol. *28*, 2125–2137.

Nakajima, H., Sim, F.H., Bond, J.R., and Unni, K.K. (1997). Small cell osteosarcoma of bone. Review of 72 cases. Cancer *79*, 2095–2106.

Noguera, R., Navarro, S., and Triche, T.J. (1990). Translocation (11;22) in small cell osteosarcoma. Cancer Genet. Cytogenet. *45*, 121–124.

Ohnishi, K., Semi, K., Yamamoto, T., Shimizu, M., Tanaka, A., Mitsunaga, K., Okita, K., Osafune, K., Arioka, Y., Maeda, T., et al. (2014). Premature termination of reprogramming in vivo leads to cancer development through altered epigenetic regulation. Cell *156*, 663–677.

Oshima, Y., Kawaguchi, S., Nagoya, S., Wada, T., Kokai, Y., Ikeda, T., Nogami, S., Oya, T., and Hirayama, Y. (2004). Abdominal small round cell tumor with osteoid and EWS/FLI1. Hum. Pathol. *35*, 773–775.

Postel-Vinay, S., Veron, A.S., Tirode, F., Pierron, G., Reynaud, S., Kovar, H., Oberlin, O., Lapouble, E., Ballet, S., Lucchesi, C., et al. (2012). Common variants near TARDBP and EGR2 are associated with susceptibility to Ewing sarcoma. Nat. Genet. *44*, 323–327.

Raouf, A., and Seth, A. (2000). Ets transcription factors and targets in osteogenesis. Oncogene *19*, 6455–6463.

Reya, T., Morrison, S.J., Clarke, M.F., and Weissman, I.L. (2001). Stem cells, cancer, and cancer stem cells. Nature *414*, 105–111.

Riggi, N., Cironi, L., Provero, P., Suva, M.L., Kaloulis, K., Garcia-Echeverria, C., Hoffmann, F., Trumpp, A., and Stamenkovic, I. (2005). Development of Ewing's sarcoma from primary bone marrow-derived mesenchymal progenitor cells. Cancer Res. *65*, 11459–11468.

Riggi, N., Suva, M.L., Suva, D., Cironi, L., Provero, P., Tercier, S., Joseph, J.M., Stehle, J.C., Baumer, K., Kindler, V., et al. (2008). EWS-FLI-1 expression triggers a Ewing's sarcoma initiation program in primary human mesenchymal stem cells. Cancer Res. *68*, 2176–2185.

Riggi, N., Knoechel, B., Gillespie, S.M., Rheinbay, E., Boulay, G., Suva, M.L., Rossetti, N.E., Boonseng, W.E., Oksuz, O., Cook, E.B., et al. (2014). EWS-FLI1 utilizes divergent chromatin remodeling

mechanisms to directly activate or repress enhancer elements in Ewing sarcoma. Cancer Cell *26*, 668–681.

Righi, A., Gambarotti, M., Longo, S., Benini, S., Gamberi, G., Cocchi, S., Vanel, D., Picci, P., Bertoni, F., Simoni, A., et al. (2015). Small cell osteosarcoma: clinicopathologic, immunohistochemical, and molecular analysis of 36 cases. Am. J. Surg. Pathol. *39*, 691–699.

Rossi, D.J., and Weissman, I.L. (2006). Pten, tumorigenesis, and stem cell self-renewal. Cell *125*, 229–231.

Selvanathan, S.P., Graham, G.T., Erkizan, H.V., Dirksen, U., Natarajan, T.G., Dakic, A., Yu, S., Liu, X., Paulsen, M.T., Ljungman, M.E., et al. (2015). Oncogenic fusion protein EWS-FLI1 is a network hub that regulates alternative splicing. Proc. Natl. Acad. Sci. USA *112*, E1307–E1316.

Semi, K., and Yamada, Y. (2015). iPS cell technology for dissecting the cancer epigenome. Cancer Sci. *106*, 1251–1256.

Shen, L., Shao, N., Liu, X., and Nestler, E. (2014). ngs.plot: quick mining and visualization of next-generation sequencing data by integrating genomic databases. BMC Genomics *15*, 284.

Smith, R., Owen, L.A., Trem, D.J., Wong, J.S., Whangbo, J.S., Golub, T.R., and Lessnick, S.L. (2006). Expression profiling of EWS/FLI identifies NKX2.2 as a critical target gene in Ewing's sarcoma. Cancer Cell *9*, 405–416.

Soldner, F., Hockemeyer, D., Beard, C., Gao, Q., Bell, G.W., Cook, E.G., Hargus, G., Blak, A., Cooper, O., Mitalipova, M., et al. (2009). Parkinson's disease patient-derived induced pluripotent stem cells free of viral reprogramming factors. Cell *136*, 964–977.

Takahashi, K., and Yamanaka, S. (2006). Induction of pluripotent stem cells from mouse embryonic and adult fibroblast cultures by defined factors. Cell *126*, 663–676.

Tanaka, M., Yamazaki, Y., Kanno, Y., Igarashi, K., Aisaki, K., Kanno, J., and Nakamura, T. (2014). Ewing's sarcoma precursors are highly enriched in embryonic osteochondrogenic progenitors. J. Clin. Invest. *124*, 3061–3074.

Tanaka, M., Yamaguchi, S., Yamazaki, Y., Kinoshita, H., Kuwahara, K., Nakao, K., Jay, P.Y., Noda, T., and Nakamura, T. (2015). Somatic chromosomal translocation between Ewsr1 and Fli1 loci leads to dilated cardiomyopathy in a mouse model. Sci. Rep. *5*, 7826.

Thomas, D.M., Johnson, S.A., Sims, N.A., Trivett, M.K., Slavin, J.L., Rubin, B.P., Waring, P., McArthur, G.A., Walkley, C.R., Holloway, A.J., et al. (2004). Terminal osteoblast differentiation, mediated by runx2 and p27KIP1, is disrupted in osteosarcoma. J. Cell Biol. *167*, 925–934.

Tirode, F., Laud-Duval, K., Prieur, A., Delorme, B., Charbord, P., and Delattre, O. (2007). Mesenchymal stem cell features of Ewing tumors. Cancer Cell *11*, 421–429.

Tirode, F., Surdez, D., Ma, X., Parker, M., Le Deley, M.C., Bahrami, A., Zhang, Z., Lapouble, E., Grossetete-Lalami, S., Rusch, M., et al. (2014). Genomic landscape of Ewing sarcoma defines an aggressive subtype with co-association of STAG2 and TP53 mutations. Cancer Discov. *4*, 1342–1353.

Torchia, E.C., Boyd, K., Rehg, J.E., Qu, C., and Baker, S.J. (2007). EWS/FLI-1 induces rapid onset of myeloid/erythroid leukemia in mice. Mol. Cell Biol. *27*, 7918–7934.

Yamada, K., Ohno, T., Aoki, H., Semi, K., Watanabe, A., Moritake, H., Shiozawa, S., Kunisada, T., Kobayashi, Y., Toguchida, J., et al. (2013). EWS/ATF1 expression induces sarcomas from neural crest-derived cells in mice. J. Clin. Invest. *123*, 600–610.

Yamashita, A., Morioka, M., Kishi, H., Kimura, T., Yahara, Y., Okada, M., Fujita, K., Sawai, H., Ikegawa, S., and Tsumaki, N. (2014). Statin treatment rescues FGFR3 skeletal dysplasia phenotypes. Nature *513*, 507–511.

Zhang, Y., Liu, T., Meyer, C.A., Eeckhoute, J., Johnson, D.S., Bernstein, B.E., Nusbaum, C., Myers, R.M., Brown, M., Li, W., et al. (2008). Model-based analysis of ChIP-seq (MACS). Genome Biol. *9*, R137.

Stem Cell Reports, Volume *6*

Supplemental Information

An *EWS-FLI1*-Induced Osteosarcoma Model Unveiled a Crucial Role of Impaired Osteogenic Differentiation on Osteosarcoma Development

Shingo Komura, Katsunori Semi, Fumiaki Itakura, Hirofumi Shibata, Takatoshi Ohno, Akitsu Hotta, Knut Woltjen, Takuya Yamamoto, Haruhiko Akiyama, and Yasuhiro Yamada

Figure S1

A

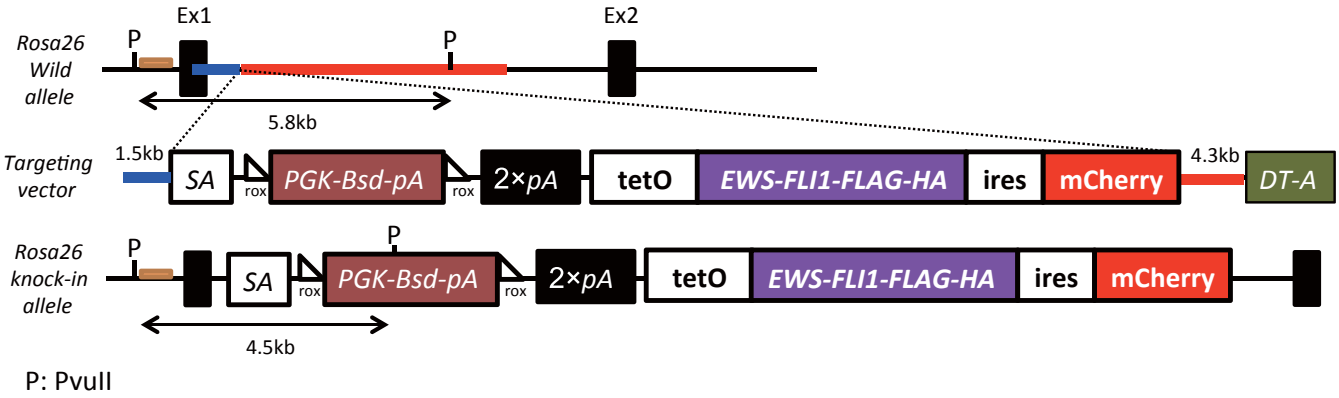

B

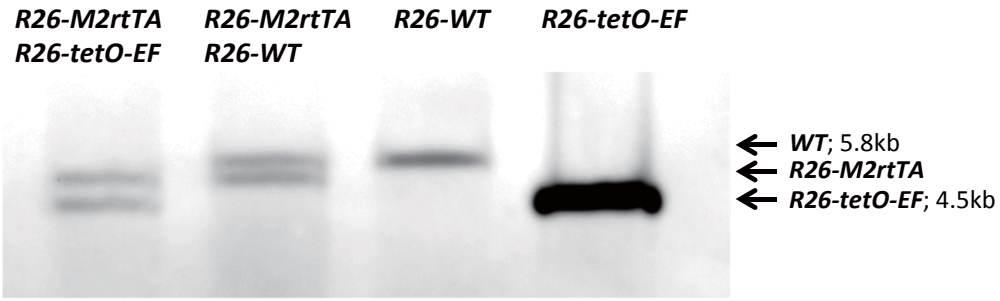

C

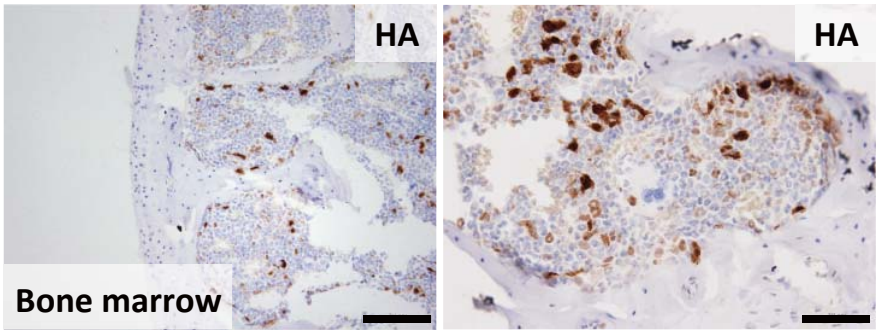

D

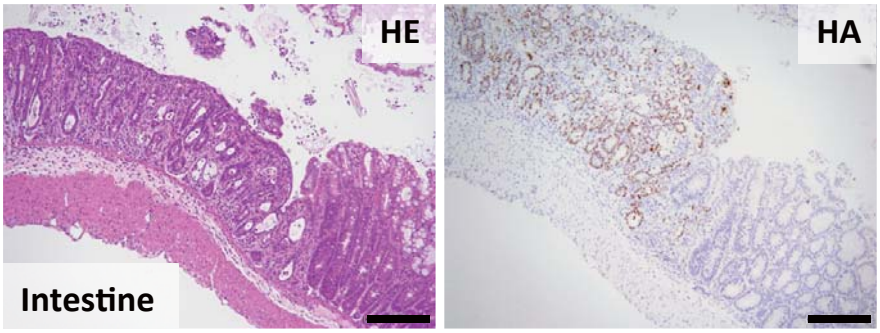

Figure S2

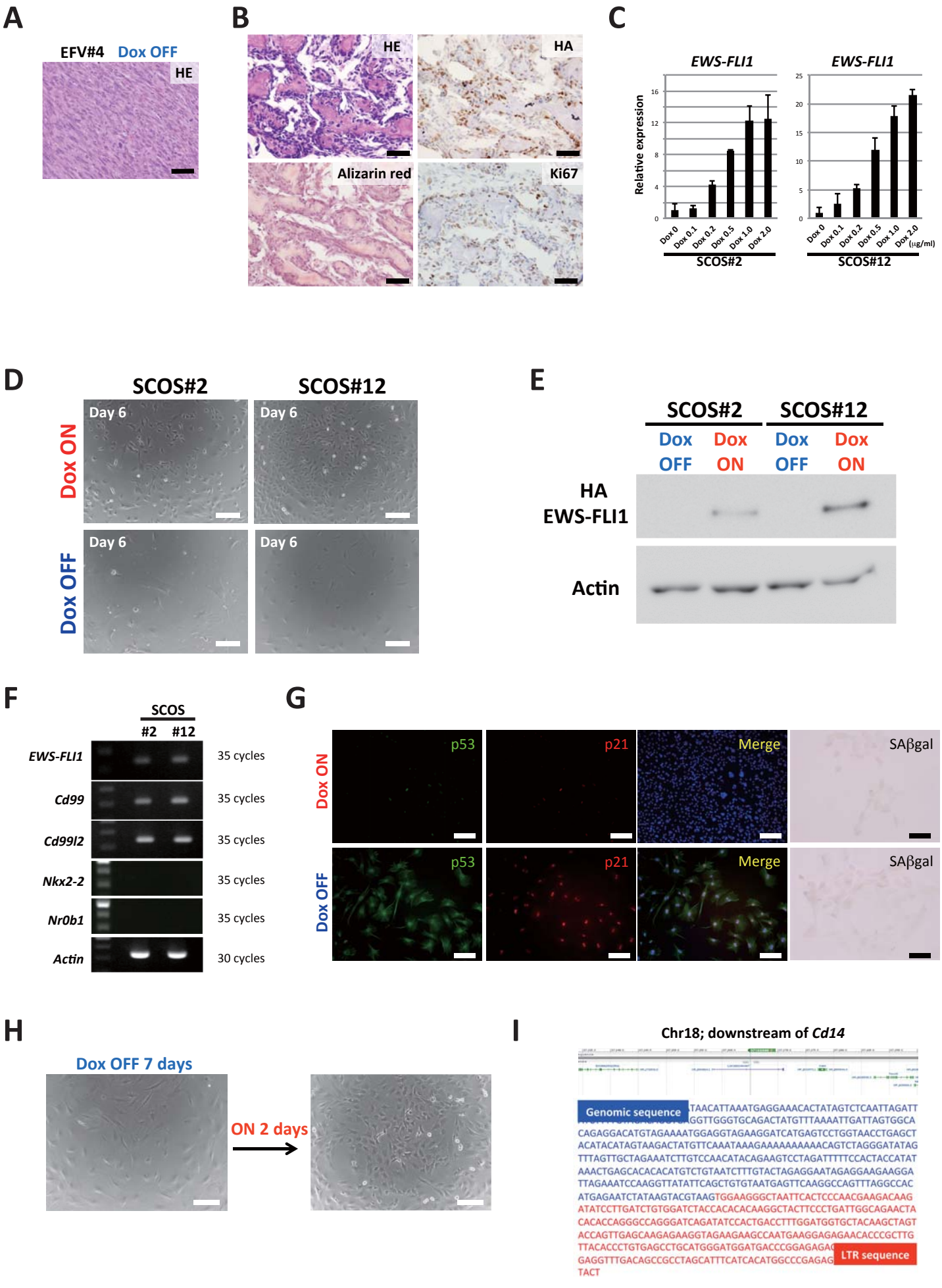
A
EFV#4 Dox OFF
HE
B
HE
HA
Alizarin red
Ki67
C
EWS-FLI1
EWS-FLI1
Relative expression
Dox 0
Dox 0.1
Dox 0.2
Dox 0.5
Dox 1.0
Dox 2.0
(μg/ml)
SCOS#2
SCOS#12
D
SCOS#2
SCOS#12
Dox ON
Dox OFF
Day 6
E
SCOS#2
SCOS#12
Dox OFF
Dox ON
HA
EWS-FLI1
Actin
F
SCOS
#2
#12
EWS-FLI1
Cd99
Cd99l2
Nkx2-2
Nr0b1
Actin
35 cycles
30 cycles
G
Dox ON
Dox OFF
p53
p21
Merge
SAβgal
H
Dox OFF 7 days
ON 2 days
I
Chr18; downstream of Cd14
Genomic sequence
LTR sequence

Figure S3

A

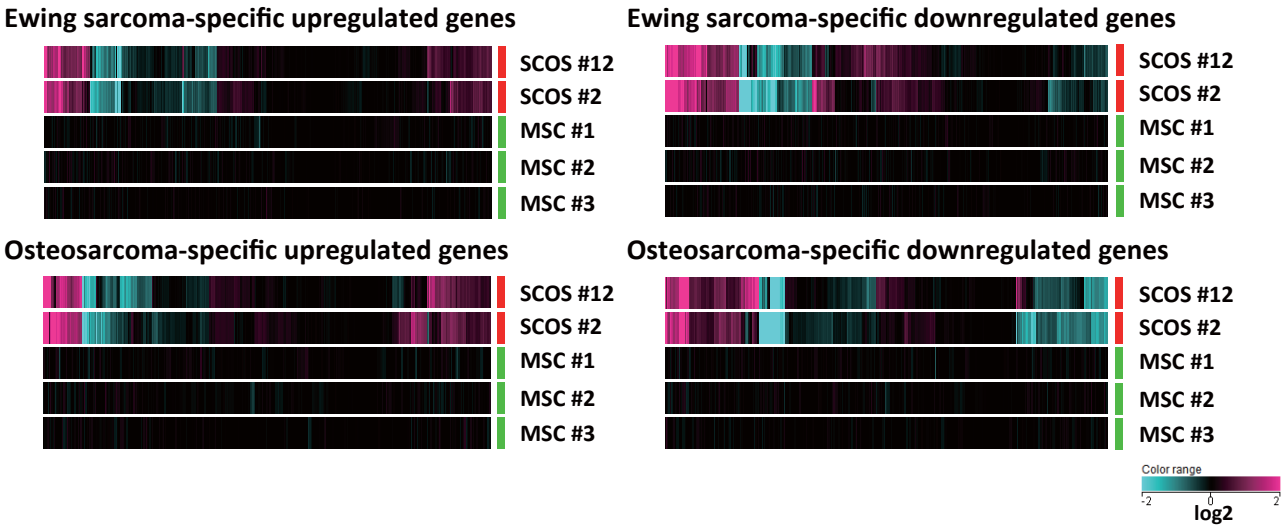

B

GO ACCESSION	GO Term	corrected p-value
GO:0005576	extracellular region	1.06E-21
GO:0044421	extracellular region part	2.16E-16
GO:0005615	extracellular space	9.86E-08
GO:0031012	extracellular matrix	7.89E-07
GO:0006950	response to stress	2.18E-05
GO:0006955	immune response	3.68E-05

C

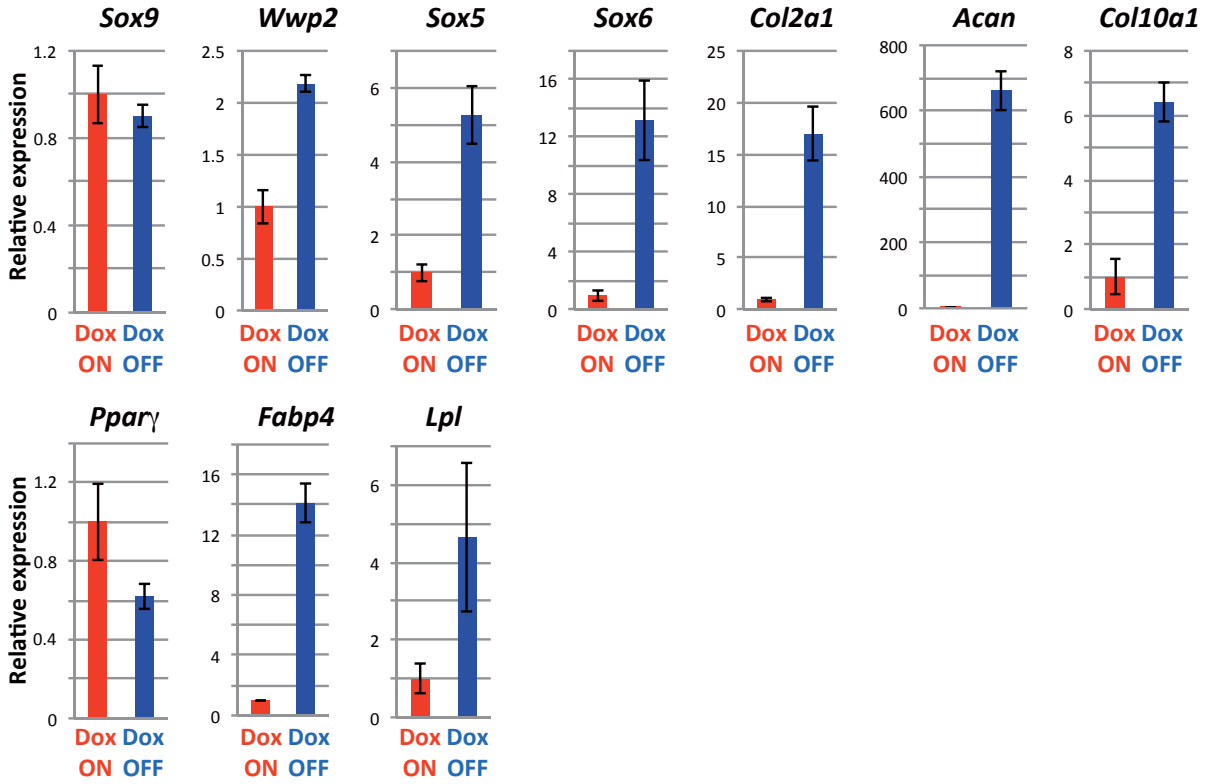

D

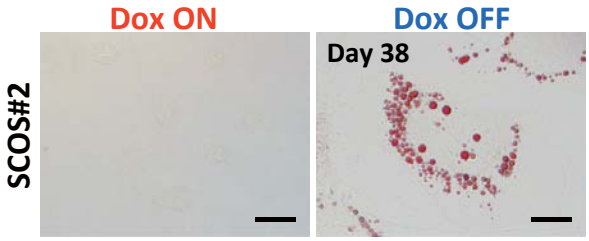

A

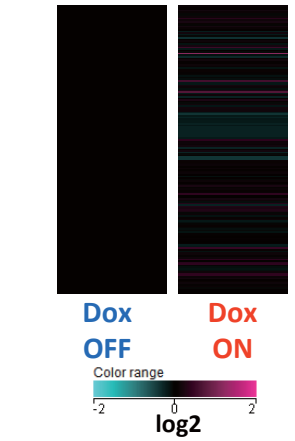

B

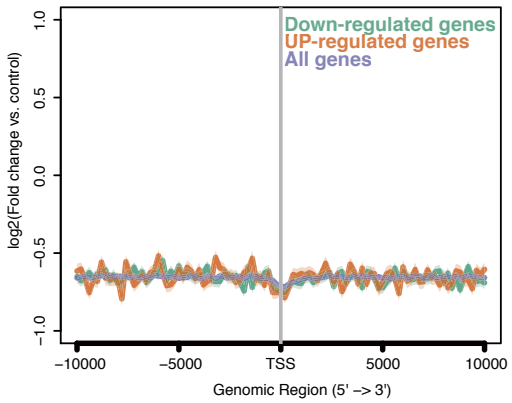

C

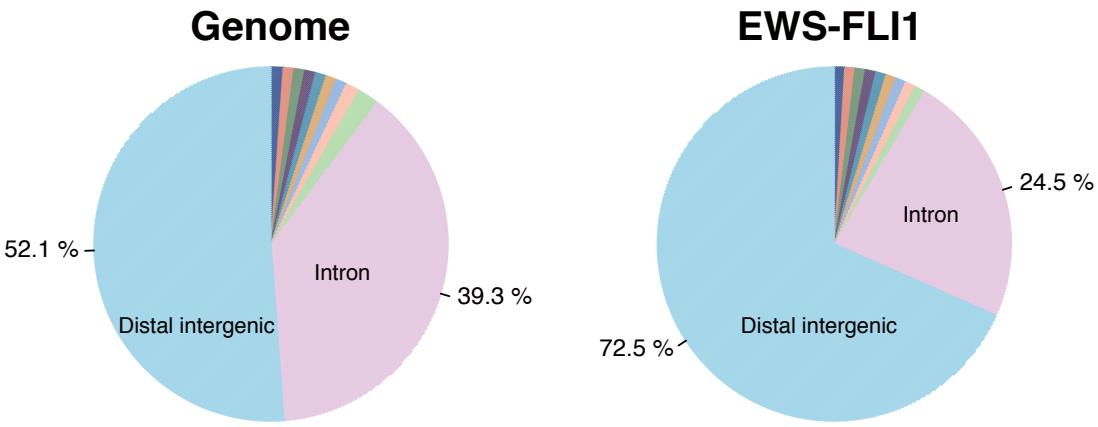

- Promoter (<=1000 bp): 1.1 %
- Promoter (1000–2000 bp): 0.8 %
- Promoter (2000–3000 bp): 0.7 %
- Downstream (<=1000 bp): 1.0 %
- Downstream (1000–2000 bp): 0.8 %
- Downstream (2000–3000 bp): 0.7 %
- 5'UTR: 0.3 %
- 3'UTR: 1.3 %
- Coding exon: 2.0 %
- Intron: 39.3 %
- Distal intergenic: 52.1 %

- Promoter (<=1000 bp): 0.2 %
- Promoter (1000–2000 bp): 0.4 %
- Promoter (2000–3000 bp): 0.5 %
- Downstream (<=1000 bp): 0.3 %
- Downstream (1000–2000 bp): 0.3 %
- Downstream (2000–3000 bp): 0.4 %
- 5'UTR: 0.1 %
- 3'UTR: 0.2 %
- Coding exon: 0.5 %
- Intron: 24.5 %
- Distal intergenic: 72.5 %

D

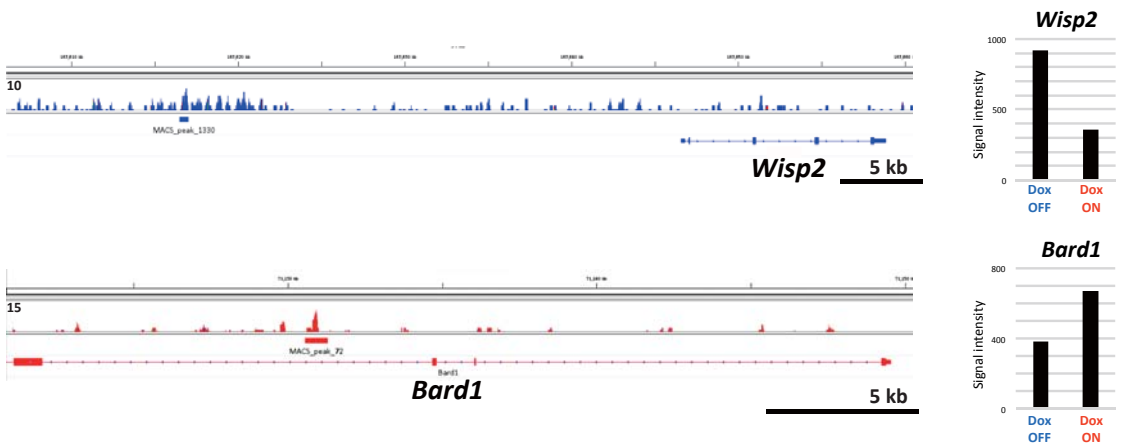

Figure S5

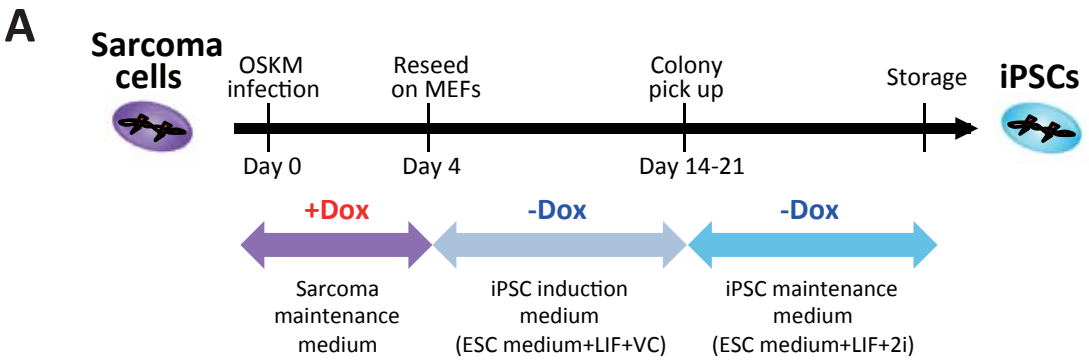
A
Sarcoma cells
OSKM infection
Reseed on MEFs
Colony pick up
Storage
iPSCs
Day 0
Day 4
Day 14-21
+Dox
-Dox
-Dox
Sarcoma maintenance medium
iPSC induction medium (ESC medium+LIF+VC)
iPSC maintenance medium (ESC medium+LIF+2i)

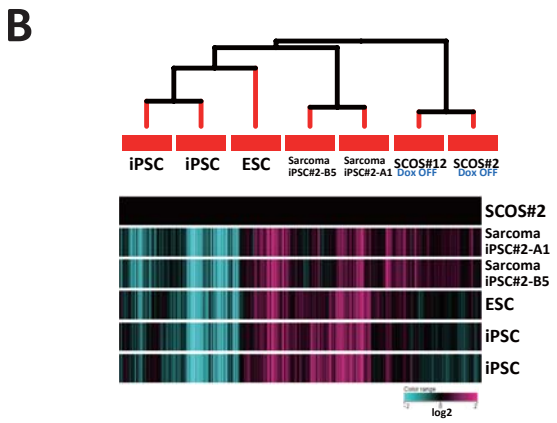
B
iPSC
iPSC
ESC
Sarcoma iPSC#2-B5
Sarcoma iPSC#2-A1
SCOS#12 Dox OFF
SCOS#2 Dox OFF
SCOS#2
Sarcoma iPSC#2-A1
Sarcoma iPSC#2-B5
ESC
iPSC
iPSC
log2

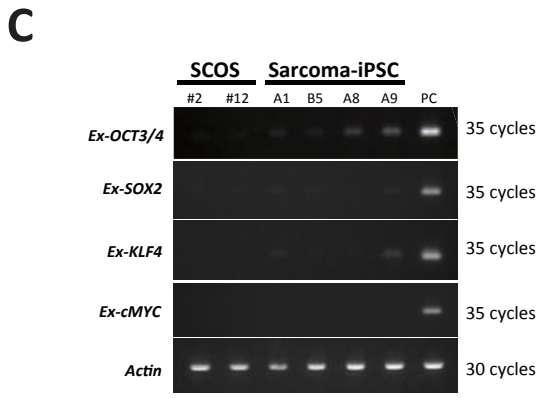
C
SCOS
Sarcoma-iPSC
#2
#12
A1
B5
A8
A9
PC
Ex-OCT3/4
Ex-SOX2
Ex-KLF4
Ex-cMYC
Actin
35 cycles
35 cycles
35 cycles
35 cycles
30 cycles

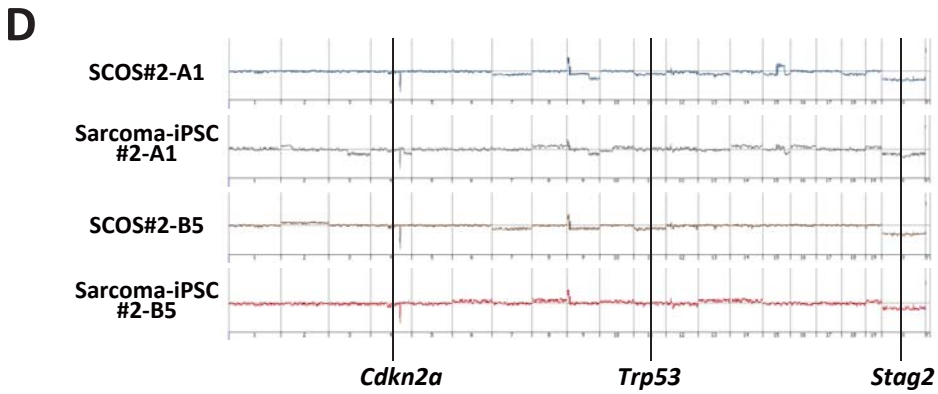
D
SCOS#2-A1
Sarcoma-iPSC #2-A1
SCOS#2-B5
Sarcoma-iPSC #2-B5
Cdkn2a
Trp53
Stag2

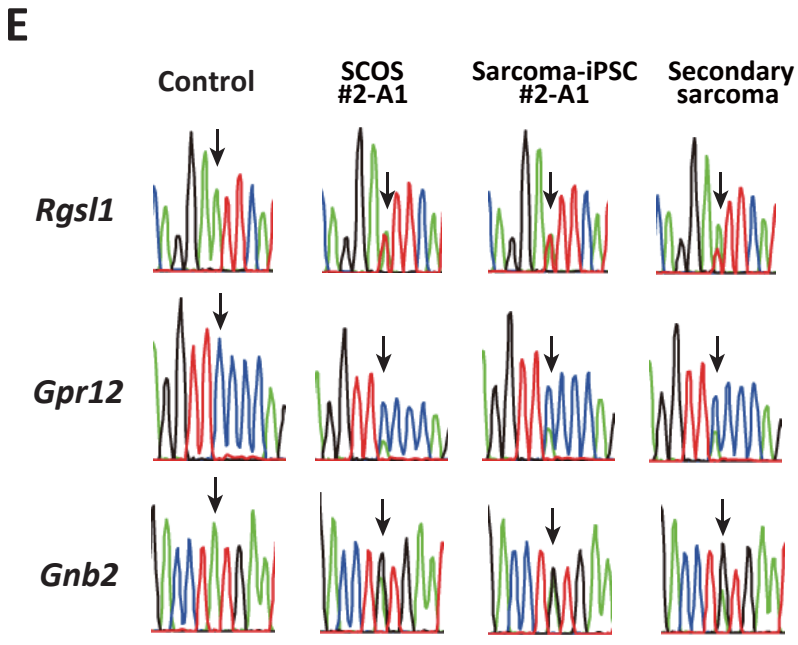
E
Control
SCOS #2-A1
Sarcoma-iPSC #2-A1
Secondary sarcoma
Rgsl1
Gpr12
Gnb2

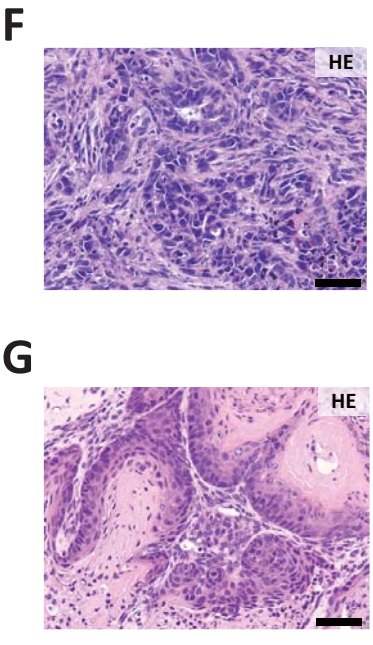
F
HE
G
HE

Table S1. Chimerism of examined mice

	Chimerism		
Genotype	Low (<30%)	Middle (30–60%)	High (>60%)
Rosa/Rosa	6	3	0
Rosa/Col	0	4	10
Total	6	7	10

Table S2. Candiate sites for unique missense mutation to *EWS-FLI1*-induced sarcoma model

Chr.	position (mm10)	REF	ALT	Gene symbol
chr1	26687331	A	G	4931408C20Rik
chr1	36419760	C	G	Fer1l5
chr1	78665011	G	A	Utp14b
chr1	85257408	C	T	C130026I21Rik
chr1	88055581	A	G	Ugt1a10
chr1	88055613	G	A	Ugt1a10
chr1	88056307	A	G	Ugt1a10
chr1	88256544	G	A	Mroh2a
chr1	153822346	A	T	Rgsl1
chr1	166146689	G	C	Gpa33
chr1	174836790	T	A	Grem2
chr2	37790432	C	G	Crb2
chr2	65098194	G	T	Cobll1
chr3	15548853	G	T	Sirpb1b
chr3	15548938	T	C	Sirpb1b
chr3	55783786	C	T	Mab21l1
chr3	108467915	G	A	5330417C22Rik
chr3	122936000	G	A	Usp53
chr4	40167087	C	T	Aco1
chr4	49792844	T	G	Grin3a
chr4	88571364	T	G	Ifna14
chr4	88816602	C	G	Ifna7
chr4	88835585	C	G	Ifna5
chr4	88835765	G	C	Ifna5
chr4	112835029	C	T	Skint6
chr4	112835089	T	A	Skint6
chr4	112872460	T	G	Skint6
chr4	112883687	C	A	Skint6
chr4	112894857	T	C	Skint6
chr4	113236373	G	T	Skint6
chr4	113238077	T	C	Skint6
chr4	113597739	C	A	Skint5
chr4	113691069	C	G	Skint5
chr4	113731063	T	A	Skint5
chr4	113827869	T	C	Skint5
chr4	113870717	C	T	Skint5
chr4	113923340	T	A	Skint5
chr4	113931810	C	G	Skint5
chr4	115762250	T	C	Efcab14
chr4	118917362	T	C	Olfr1329
chr4	134082593	C	T	Aim1l
chr4	147390321	A	G	Gm13145
chr4	156350965	T	C	Gm20782
chr5	87694785	C	T	Csn2
chr5	104065104	G	A	Nudt9
chr5	137529034	A	G	Gnb2
chr5	138240988	G	A	Nxpe5
chr5	146583613	C	A	Gpr12
chr6	97184820	T	A	Uba3
chr6	128357780	G	A	Rhno1
chr6	128357786	G	A	Rhno1
chr6	128357832	A	G	Rhno1
chr6	128357852	G	A	Rhno1
chr7	43225856	A	G	EU599041
chr7	48552900	G	T	Mrgprb2
chr7	97501779	T	A	Ints4
chr7	106677718	T	A	Olfr693
chr7	138836628	G	A	Mapk1ip1
chr7	140345816	G	T	Olfr60
chr8	17534910	C	T	Csmd1
chr8	36584125	T	C	Dlc1
chr8	110883353	C	T	Fuk
chr9	48450414	G	A	Gm5616
chr9	48450432	C	T	Gm5616
chr9	108955787	C	A	Col7a1
chr10	86905643	C	G	Stab2
chr11	58625248	G	A	Olfr323
chr11	58625303	C	G	Olfr323
chr11	58625761	G	A	Olfr323
chr11	58625792	T	G	Olfr323
chr11	58625905	A	C	Olfr323
chr11	58683931	G	T	Olfr320
chr11	58684256	G	A	Olfr320
chr11	58684462	C	T	Olfr320

chr11	58684714	G	A	Olfr320
chr11	58684721	T	C	Olfr320
chr11	58701957	A	C	Olfr319
chr11	58702326	C	T	Olfr319
chr11	58702395	C	A	Olfr319
chr11	58732373	T	G	Olfr317
chr11	58732648	T	C	Olfr317
chr11	58757966	G	A	Olfr316
chr11	58758068	C	T	Olfr316
chr11	58758104	A	G	Olfr316
chr11	58786946	A	G	Olfr314
chr11	116769067	G	T	St6galnac1
chr12	64473027	T	G	Fscb
chr12	76329274	T	C	Akap5
chr12	101418121	C	A	Catsperb
chr12	103693807	G	T	Serpina1f
chr12	104134219	G	C	Serpina3b
chr12	104340975	A	G	Serpina3k
chr12	113625541	T	C	Ighv5-6
chr12	113625945	C	A	Ighv5-6
chr12	113655233	G	C	Ighv5-8
chr12	113702423	T	A	Ighv5-12
chr12	113796269	A	T″	Ighv2-6-8
chr12	113796269	A	T″	Ighv2-6-8
chr12	113796269	A	T″	Ighv2-6-8
chr12	113796269	A	T″	Ighv2-6-8
chr12	113859405	T	G	Ighv5-17
chr12	113932083	C	T	Ighv14-1
chr12	113932196	G	A	Ighv14-1
chr12	113994755	G	T	Ighv14-2
chr12	114094228	G	A	Ighv9-1
chr12	114094229	C	T	Ighv9-1
chr12	114153426	A	T	Ighv7-3
chr12	114176681	G	A	Ighv14-4
chr12	114176691	G	A	Ighv14-4
chr12	114406948	G	T	Ighv6-4
chr12	114851275	A	T	Ighv1-34
chr12	114851307	C	T	Ighv1-34
chr12	114851322	T	A	Ighv1-34
chr12	114914615	C	T	Ighv1-39
chr12	114914857	A	T	Ighv1-39
chr12	115495818	T	G	Ighv1-63
chr12	115495858	C	T	Ighv1-63
chr12	115834373	A	G	Ighv1-75
chr12	115834392	C	G	Ighv1-75
chr12	115868845	T	G	Ighv1-78
chr13	61539620	C	T	Ctsm
chr13	61568124	C	T	Cts3
chr13	66431401	G	A	2410141K09Rik
chr13	66431419	C	T	2410141K09Rik
chr13	66431466	C	A	2410141K09Rik
chr13	66432161	G	T	2410141K09Rik
chr13	67256963	A	C	Zfp458
chr13	67256967	T	C	Zfp458
chr13	67256982	T	C	Zfp458
chr14	113315351	G	A	Tpm3-rs7
chr14	123954597	G	A	Itgbl1
chr15	73524148	G	A	Dennd3
chr15	98950656	C	G	Tuba1a
chr16	34666699	C	G	Ropn1
chr17	23311138	C	A	Vmn2r114
chr17	23311142	C	G	Vmn2r114
chr17	23346388	T	A	Vmn2r115
chr17	43064973	A	T	Tnfrsf21
chr18	12402904	A	T	Lama3
chr18	60269984	G	T	Gm4841
chr18	60270026	C	A	Gm4841
chr18	60270033	A	T	Gm4841
chr18	60270097	C	T	Gm4841
chr19	13410580	T	G	Olfr1469
chr19	37916431	C	T	Myof
chrX	7163391	C	A	Clcn5
chrX	21083065	A	T	Zfp300

Table S3. Overlapping mutations in murine *EWS–FLI1* sarcoma model and human sarcomas (Ewing sarcomas/PNETs and osteosarcomas)

Unique missense mutations in *EWS–FLI1*–induced sarcoma model		**Human Ewings sarcoma–peripheral primitive neuroectodermal tumour**		**Human osteosarcoma**	
Mouse gene symbol	Human gene symbol	Mutated samples (frequency) N=342	Detailed information	Mutated samples (frequency) N=58	Detailed information
Csmd1	CSMD1 (ENST00000537824)	15 (4.4%)	506 c.1518G>A p.S506S COSM1456746 1 Substitution – coding silent 1168 c.3502C>T p.R1168C COSM5030424 1 Substitution – Missense 1312 c.3934C>G p.P1312A COSM5030038 1 Substitution – Missense 1455 c.4365G>T p.L1455L COSM4588054 1 Substitution – coding silent 1533 c.4599C>T p.S1533S COSM1099201 1 Substitution – coding silent 1754 c.5260G>A p.G1754S COSM5029552 1 Substitution – Missense 1877 c.5631A>G p.V1877V COSM4588044 1 Substitution – coding silent 2138 c.6412C>T p.P2138S COSM4588042 1 Substitution – Missense 2220 c.6660A>T p.T2220T COSM4588040 1 Substitution – coding silent 2224 c.6672G>A p.T2224T COSM2789183 1 Substitution – coding silent 2340 c.7020T>A p.N2340K COSM5029445 1 Substitution – Missense 2760 c.8278G>A p.V2760M COSM4588034 1 Substitution – Missense 2807 c.8419C>T p.R2807C COSM274673 1 Substitution – Missense 2879 c.8635G>A p.A2879T COSM1623896 1 Substitution – Missense 2894 c.8682C>T p.N2894N COSM237253 1 Substitution – coding silent 2903 c.8709T>G p.S2903R COSM5030558 1 Substitution – Missense	4 (6.9%)	62 c.186C>T p.I62I COSM5023630 1 Substitution – coding silent 524 c.1570A>G p.K524E COSM5021556 1 Substitution – Missense 1774 c.5320C>A p.Q1774K COSM5024049 1 Substitution – Missense ? c.2593+3G>C p.? COSM5024485 1 Unknown
Col7a1	COL7A1	9 (2.6%)	327 c.979G>T p.A327S COSM4584435 1 Substitution – Missense 469 c.1405T>C p.Y469H COSM4584434 1 Substitution – Missense 593 c.1777C>T p.R593W COSM4584433 1 Substitution – Missense 1053 c.3159G>A p.A1053A COSM4584432 1 Substitution – coding silent 1156 c.3468C>T p.H1156H COSM4584431 1 Substitution – coding silent 1225 c.3673G>C p.A1225P COSM4584430 1 Substitution – Missense 1523 c.4567C>A p.P1523T COSM5030007 1 Substitution – Missense 2177 c.6527_6528insC p.G2177Tfs*113 COSM4584429 1 Insertion – Frameshift 2859 c.8575T>G p.S2859A COSM4584428 1 Substitution – Missense	N.D.	
Grin3a	GRIN3A	5 (1.5%)	493 c.1478A>T p.Y493F COSM3167357 1 Substitution – Missense 634 c.1902C>T p.I634I COSM4588303 1 Substitution – coding silent 708 c.2123G>A p.R708Q COSM3167342 1 Substitution – Missense 975 c.2925C>T p.T975T COSM5030015 1 Substitution – coding silent 1085 c.3254A>T p.Q1085L COSM4588302 1 Substitution – Missense	3 (5.2%)	554 c.1660T>C p.L554L COSM3982644 1 Substitution – coding silent 594 c.1781A>T p.D594V COSM1732353 1 Substitution – Missense 607 c.1821A>C p.A607A COSM3982643 1 Substitution – coding silent 1065 c.3194C>T p.A1065V COSM5023025 1 Substitution – Missense
Dennd3	DENND3	3 (0.9%)	449 c.1346C>T p.P449L COSM604520 1 Substitution – Missense 542 c.1626C>T p.S542S COSM4587797 1 Substitution – coding silent 974 c.2922C>A p.H974Q COSM4587798 1 Substitution – Missense 975 c.2923A>G p.S975G COSM4587799 1 Substitution – Missense	1 (1.7%)	363 c.1087C>T p.L363L COSM5021567 1 Substitution – coding silent
Dlc1	DLC1	3 (0.9%)	617 c.1850G>A p.R617Q COSM1096059 1 Substitution – Missense 651 c.1951T>C p.F651L COSM4587773 1 Substitution – Missense 1055 c.3163A>G p.S1055G COSM1250143 1 Substitution – Missense	N.D.	
Lama3	LAMA3	3 (0.9%)	1556 c.4668G>A p.P1556P COSM4580342 1 Substitution – coding silent 2672 c.8016C>T p.D2672D COSM2807632 1 Substitution – coding silent ? c.5112+1G>A p.? COSM4580344 1 Unknown	N.D.	
Myof	MYOF	3 (0.9%)	366 c.1096C>T p.R366* COSM4573900 1 Substitution – Nonsense 662 c.1984G>A p.A662T COSM4573897 1 Substitution – Missense 714 c.2142C>T p.N714N COSM3397310 1 Substitution – coding silent	N.D.	
Ugt1a10	UGT1A10	2 (0.6%)	50 c.150C>T p.L50L COSM3050195 1 Substitution – coding silent 374 c.1122T>C p.G374G COSM4583326 1 Substitution – coding silent	N.D.	
Crb2	CRB2	2 (0.6%)	93 c.277C>T p.R93C COSM4588458 1 Substitution – Missense 104 c.310C>T p.R104C COSM4588460 1 Substitution – Missense	N.D.	
Stab2	STAB2	2 (0.6%)	1041 c.3123C>T p.D1041D COSM4574950 1 Substitution – coding silent 1968 c.5903C>A p.A1968D COSM4574951 1 Substitution – Missense 2374 c.7121G>A p.R2374Q COSM4574953 1 Substitution – Missense	N.D.	
St6galnac1	ST6GALNAC1	2 (0.6%)	277 c.831G>A p.T277T COSM4580166 1 Substitution – coding silent 387 c.1159G>A p.D387N COSM4580165 1 Substitution – Missense	N.D.	
5330417C22Rik	KIAA1324	2 (0.6%)	351 c.1052T>C p.M351T COSM4576078 1 Substitution – Missense 898 c.2690_2691delAG p.R898fs*56 COSM4576079 1 Deletion – Frameshift	N.D.	
Aco1	ACO1	1 (0.3%)	876 c.2628C>T p.N876N COSM4588759 1 Substitution – coding silent	1 (1.7%)	630 c.1889C>T p.S630L COSM5024313 1 Substitution – Missense
Akap5	AKAP5	1 (0.3%)	350 c.1050T>C p.F350F COSM4577961 1 Substitution – coding silent	1 (1.7%)	184 c.550G>A p.E184K COSM1300753 1 Substitution – Missense
Clcn5	CLCN5	1 (0.3%)	460 c.1380T>A p.A460A COSM4589464 1 Substitution – coding silent	1 (1.7%)	390 c.1169A>C p.N390T COSM5023942 1 Substitution – Missense
Tnfrsf21	TNFRSF21	1 (0.3%)	48 c.144G>A p.S48S COSM1079994 1 Substitution – coding silent	1 (1.7%)	483 c.1447C>T p.R483C COSM5024184 1 Substitution – Missense
Zfp458	ZNF43	1 (0.3%)	717 c.2150G>A p.R717Q COSM4580861 1 Substitution – Missense	1 (1.7%)	737 c.2209G>A p.E737K COSM5022020 1 Substitution – Missense
Cobll1	COBLL1	1 (0.3%)	973 c.2917G>A p.D973N COSM5030279 1 Substitution – Missense	N.D.	
Mab21l1	MAB21L1	1 (0.3%)	244 c.731G>A p.G244E COSM4575915 1 Substitution – Missense	N.D.	
Aim1l	AIM1L	1 (0.3%)	558 c.1674G>T p.E558D COSM4577167 1 Substitution – Missense	N.D.	
Gnb2	GNB2	1 (0.3%)	291 c.871_880del10 p.D291fs*7 COSM3080668 1 Deletion – Frameshift	N.D.	
Catsperb	CATSPERB	1 (0.3%)	41 c.122C>T p.P41L COSM4578062 1 Substitution – Missense	N.D.	
Itgbl1	ITGBL1	1 (0.3%)	365 c.1093G>T p.D365Y COSM4575812 1 Substitution – Missense	N.D.	
Ifna5 Ifna7 Ifna14	IFNA4	1 (0.3%)	60 c.179G>C p.G60A COSM4588738 1 Substitution – Missense	N.D.	
Mrgprb2	MRGPRX1	1 (0.3%)	245 c.733G>T p.D245Y COSM4574247 1 Substitution – Missense	N.D.	
Olfr314	OR2T8	1 (0.3%)	56 c.167C>T p.P56L COSM2232658 1 Substitution – Missense	N.D.	
Zfp300	ZNF567	1 (0.3%)	409 c.1225_1233delGAGAAA... p.E409_T411delEKT COSM5030662 1 Deletion – In frame	N.D.	
Gpa33	GPA33	N.D.		1 (1.7%)	138 c.413T>C p.L138P COSM5023795 1 Substitution – Missense
Fscb	FSCB	N.D.		1 (1.7%)	805 c.2414C>T p.A805V COSM5023103 1 Substitution – Missense
Olfr323	OR11L1	N.D.		1 (1.7%)	217 c.650C>G p.P217R COSM5023988 1 Substitution – Missense

N.D.; not detected

Table S4. Primer sequence

	Genes	Forward (5' ⇒ 3')	Reverse (5' ⇒ 3')	
qRT-PCR	*EWS-FLI*	CAATATAGCCAACAGAGCAGCAG	CTCCAAGGGGAGGACTTTTG	
	Nanog	TGCTTACAAGGGTCTGCTACTG	TAGAAGAATCAGGGCTGCCTTG	
	Oct3/4 (endogenous)	TCCCATGCATTCAAACTGAG	CCACCCCTGTTGTGCTTTTA	(Ohnishi, Semi et al. 2014)
	Runx2	ACAGTCCCAACTTCCTGTGC	TTCTCATCATTCCCGGCCATG	
	Sp7	TTCTCTCCATCTGCCTGACTCC	GCTAGAGCCGCCAAATTTGC	
	Col1a1	TGGCGGTTATGACTTCAGCTTCCT	GGTCACGAACCACGTTAGCATCAT	
	Pth1r	CCAACTACAGCGAGTGCCTC	GGTGAGGGAGGCAAGAGACA	
	Bglap	AGTGTGAGCTTAACCCTGCTTG	ATGCGTTTGTAGGCGGTCTTC	
	Dmp1	TGATTTGGCTGGGTCACCAC	TGTCCGTGTGGTCACTATTTGC	
	Sost	AGAACAACCAGACCATGAACCG	TGTACTCGGACACATCTTTGGC	
	Fgf23	CCACGGCAACATTTTTGGATCG	TGCGACAAGTAGACGTCATAGC	
	Mepe	ATGAAGATGCAGGCTGTGTCTG	AGATGCTGCCAAGTCCTTGTG	
	Sox9	GCAAGCTGGCAAAGTTGATCTG	ACGTCGAAGGTCTCAATGTTGG	
	Wwp2	AAGTGGAGCGGAGTTAGGC	AAGCTGGGACTTCTCAAAAGG	
	Sox5	CTTTCCCGACATGCACAATTCC	TACTTCTCCAGGTGCTGTTTGC	
	Sox6	ATGGCAAGAAGCTCCGGATTG	AACACCTGTTCCTGTGGTGATG	
	Col2a1	CCAAACACTTTCCAACCGCAGTCA	AGTCTGCCCAGTTCAGGTCTCTTA	
	Acan	TTCACTGTAACCCGTGGACT	TGGTCCTGTCTTCTTTCAGC	
	Col10a1	ATAGGCAGCAGCATTACGAC	TAGGCGTGCCGTTCTTATAC	
	Pparg	GCTGTGAAGTTCAATGCACTGG	TGCAGCAGGTTGTCTTGGATG	
	Fabp4	ATGAAATCACCGCAGACGACAG	ATTGTGGTCGACTTTCCATCCC	
	Lpl	AGCCAAGAGAAGCAGCAAGATG	AAATCTCGAAGGCCTGGTTGTG	
	Actb	GCCAACCGTGAAAAGATGAC	TCCGGAGTCCATCACAATG	
RT-PCR	*Cd99*	AAGGCCACACGGAGACTCAG	TGATAGGCCACGAAGCTCGA	
	Cd99l2	TCAGCACCACGACTAGGAGG	GTATCCCCCACCTTCCACGA	
	Nkx2-2	ACCAACACAAAGACGGGGTT	GTCATTGTCCGGTGACTCGT	
	Nr0b1	ATGGAGATCCCGGAGACCAA	GGATCTGCTGGGTTCTCCAC	
	Ex-hOCT3/4	GCTCTCCCATGCATTCAAACTGA	CTTACGCGAAATACGGGCAGACA	
	Ex-hSOX2	TTCACATGTCCCAGCACTACCAGA	GACATGGCCTGCCCGGTTATTATT	
	Ex-hKLF4	CCACCTCGCCTTACACATGAAGA	GACATGGCCTGCCCGGTTATTATT	
	Ex-h-cMYC	ATACATCCTGTCCGTCCAAGCAGA	GACATGGCCTGCCCGGTTATTATT	
	Actb	GCTACAGCTTCACCACCACA	CTTCTGCATCCTGTCAGCAA	
Bisulfite genomic sequence	*Nanog* promoter	GATTTTGTAGGTGGGATTAATTGTGAATTT	ACCAAAAAAAACCCACACTCATATCAATATA	(Takahashi and Yamanaka 2006)
	Oct3/4 distal enhancer	GGTTTTAGAGGTTGGTTTTGGG	CATCTCTCTAACCCTCTCCATAAATC	(Theunissen, Costa et al. 2011)

		5' ⇒ 3'	
Virus integration site detection	Asymmetric linker cassette LC1_adaptor	GACCCGGGAGATCTGAATTCAGTGGCACAG	
	Asymmetric linker cassette LC2_adaptor	CTGTGCCACTG	
	1st_PCR_AP1_F	GACCCGGGAGATCTGAATTC	
	1st_PCR_pSLIK1_R	GTCGAGAGAGCTCCTCTGGTTTC	(Varas, Stadtfeld et al. 2009)
	2nd_PCR_AP2_F	CCTATCCCCTGTGTGCCTTGGCAGTCTCAGGATCTGAATTCAGTGGCACAG	
	2nd_PCR_pSLIK2_R	CTTTCGCTTTCAAGTCCCTGTTCG	
	3rd_seq_LTR_R	CTCAAGGCAAGCTTTATTGAGGC	

Legends to Supplemental Figures

Figure S1; Related to Figure1. *Rosa-M2rtTA/Rosa::tetO-EWS-FLI1* system and phenotype caused by *EWS-FLI1* expression in mice.

A. Schematic representation of the *Rosa26* targeting allele. *tetO-EWS-FLI1-ires-mCherry* is inserted into intron 1 of the *Rosa26* locus. SA, splice acceptor; ires, internal ribosome entry site; pA, poly(A) sequence; DT-A, diphtheria toxin A.

B. Southern blot analysis of the Bsd resistant clone using a 5' external probe. Note that the obtained clone harbors both the *Rosa26-M2rtTA* allele and *Rosa26::tetO-EWS-FLI1* allele.

C. Anti-HA immunostaining of bone in *Rosa*::*M2rtTA/Col1a1*::*tetO-EWS-FLI1* mice. EWS-FLI1 positive cells are observed in the bone marrow after Dox treatment. Scale bars, 100 μm (left) and 50 μm (right).

D. EWS-FLI1 expressing cells exhibit dysplastic change in the intestine of *Rosa-M2rtTA/Col1a1*::*tetO-EWS-FLI1* mice. Scale bars, 200 μm.

Figure S2; Related to Figure2. Characterization of *EWS-FLI1*-dependent osteosarcoma cell lines SCOS#2 and SCOS#12.

A. EFV#4 developed spindle cell sarcomas in immunocompromised mice even in the absence of Dox. Scale bar, 50 μm.

B. *EWS-FLI1*-induced tumor (EFN#2) was negative for Alizarin red staining. Immunohistochemistry using HA and Ki67 antibody revealed that *EWS-FLI1*-induced tumor expresses EWS-FLI1 and has high proliferative activity. Scale bars, 50 μm.

C. qRT-PCR analysis shows that both SCOS#2 and SCOS#12 express *EWS-FLI1* mRNA in a Dox concentration-dependent manner (0.1-2.0 μg/ml). Data are presented as mean ± SD. The expression level of Dox 0 cells was set to 1.

D. Morphology of the *EWS-FLI1*-dependent sarcoma cell lines SCOS#2 and SCOS#12 (top). Both cell lines changed their morphology to large and flat cells 6 days after Dox withdrawal (bottom). Scale bars; 200μm.

E. The sarcoma cell lines express EWS-FLI1 protein in the presence of Dox. EWS-FLI1 protein was detected by western blotting using anti-HA antibody.

F. RT-PCR analysis shows that SCOS#2 and SCOS#12 express surface antigen *Cd99*, which is marker of human Ewing sarcoma, and its variant *Cd99l2*. However, *Nkx2-2* and *Nr0b1*, direct targets of *EWS-FLI1* in Ewing sarcoma, were undetectable, suggesting that SCOS#2 and SCOS#12 have

different properties from Ewing sarcoma.

G. Immunocytochemistry for p53 and p21. The withdrawal of Dox leads to the increased expression of p53 and p21 and to growth arrest. Senescence associated beta-galactosidase (SAβgal) activity was not observed. Scale bars, 200 μm (first three columns) and 50 μm (right column).

H. Re-administration of Dox gives proliferative potential to resting sarcoma cells, suggesting that the cell cycle arrest was induced in sarcoma cells by the withdrawal of *EWS-FLI1* expression. Scale bars; 200μm.

I. The lentivirus integration site was investigated by LM-PCR (Varas et al., 2009). The analysis identified the integration site downstream region of the *Cd14* gene.

Figure S3; Related to Figure3. Gene expression change in *EWS-FLI1*-dependent osteosarcoma cell lines

A. Expression of upregulated and downregulated genes in human Ewing sarcomas and human osteosarcomas in SCOS#2 and SCOS#12. Note that SCOSs exhibit a partial similarity with both human Ewing sarcomas and human osteosarcomas. Published microarray data of 8 human Ewing sarcomas (GSM213306, GSM213307, GSM213308, GSM213309, GSM213310, GSM510019, GSM510022 and GSM510025), 3 human MSCs (GSM906367, GSM906368 and GSM906369), 8 human osteosarcomas (GSM1349294, GSM1517387, GSM1727193, GSM1727195, GSM1727196, GSM1727197, GSM1893361 and GSM1893364) and 3 murine MSCs (GSM1180589, GSM1180590 and GSM1180591) were used (Feng et al., 2015; Grilli et al., 2015; Kawano et al., 2015; Lu et al., 2015; Mackintosh et al., 2012; Miyagawa et al., 2008; Ullah et al., 2014). For this analysis, we first extracted upregulated and downregulated genes in human Ewing sarcomas and human osteosarcomas when compared with human MSCs (two folds). Then, upregulated and downregulated genes specific to Ewing sarcoma or osteosarcoma were identified by comparing the two gene sets (two folds higher or lower in each sarcoma type), respectively. Gene symbols in a human microarray platform (GeneChip U133 Plus 2.0 Array) were converted to gene symbols in a mouse microarray platform (GeneChip Mouse Gene 1.0ST Array) and analyzed for gene expressions.

B. Gene ontology enrichment analysis showed that extracellular region and matrix-related genes are upregulated in Dox OFF (72 hrs after withdrawal) compared to Dox ON in SCOS#12. The upregulated genes were selected by a cutoff point at fold change >2.0 and p-value <1.0E-4. The top 4 enriched clusters are highlighted.

C. The increased expression of chondrogenic and adipogenic differentiation-related genes in sarcoma cells at 38 days after Dox withdrawal. mRNA expression levels were measured by qRT-PCR. Data

are presented as mean ± SD. The expression level of Dox ON cells was set to 1.

D. At 38 days after Dox withdrawal, sarcoma cells exhibited positive staining for Oil red O. Scale bars; 20μm.

Figure S4; Related to Figures 3. ChIP-seq analysis for EWS-FLI1 binding to SCOS#2.

A. Genes which possess EWS-FLI1 binding sites close to their TSS (±5 kb, 126 genes and 181 probe sets) were analyzed for their expression. No obvious difference in the expression levels was detected between Dox ON and OFF sarcomas.

B. EWS-FLI1-binding near the TSSs of upregulated/downregulated genes. No obvious enrichment was observed in either upregulated or downregulated genes.

C. The distribution of EWS-FLI1 binding sites. Right: regions of EWS-FLI1 binding to SCOS#2, Left: regions of the reference genome. EWS-FLI1 preferentially binds to the distal intergenic region of SCOS#2.

D. Representative genes (*Wisp2* and *Bard1*) dysregulated in SCOS#2. EWS-FLI1 binds at the distal intergenic region near *Wisp2* and at the intron of *Bard1*.

Figure S5; Related to Figures 4 and 5. Characterization of sarcoma-derived iPSCs and secondary sarcomas derived from these iPSCs.

A. Schematic illustration of the iPSC derivation protocol from *EWS-FLI1*-dependent osteosarcoma cells.

B. Hierarchical clustering analysis of *EWS-FLI1*-induced sarcoma, sarcoma-iPSCs and control ESCs/iPSCs (GSE45916) (Ohta et al., 2013). Comparison of global gene expressions by microarray analysis indicated that sarcoma-iPSCs have normal PSC-like gene expression patterns. Color range is shown using a log2 scale.

C. RT-PCR showed the silencing of exogenous *OCT3/4, SOX2, KLF4* and *cMYC* expression in established sarcoma-iPSC-like cells.

D. Array CGH analysis of parental sarcoma cells and the established iPSCs. Some chromosomal abnormalities are identical between sarcoma-derived iPSCs and the parental sarcoma cells. The locations of *Stag2*, *Trp53*, and *Cdkn2a*, which are common mutated genes in human Ewing sarcoma, are indicated. SCOS#2 was established from bone marrow stromal cells of male *Rosa26-M2rtTA* mouse. Genomic DNA from female C57BL/6 mice was used as reference for the CGH analysis.

E. Direct sequencing results of representative genetic mutations in sarcoma cells (SCOS#2), sarcoma-iPSCs and the secondary sarcoma, which were identified by exome analysis.

F. Secondary sarcomas derived from the sarcoma-iPSCs often contain the carcinoma component. Scale

bar, 50 μm.

G. Parakeratosis of squamous epithelium is detected in sarcoma iPSCs-derived teratomas, which implies the impairment of terminal differentiation. Scale bar, 50 μm.

Supplemental Experimental Procedures

Rosa26 targeting vector, ESC targeting and generation of chimeric mice

The *EWS-FLI1* type1 fusion gene was cloned from Ewing sarcoma cell line TC135 (Takigami et al., 2011). For the *Rosa-M2rtTA/Rosa*::*tetO-EWS-FLI1* system, the Red/ET BAC recombination system was used to introduce *TetOP-EWS-FLI1-FLAG-HA-ires-mCherry-pA* and the selection cassette (*SA-rox-PGK-EM7-BsdR-pA-rox-2pA*) into intron 1 of *Rosa26* BAC. The obtained vector was electropolated to KH2 ESCs, which had the *Rosa26-M2rtTA* allele (Beard et al., 2006). ESCs were cultured with ES media containing 15 μg/ml BlasticidinS (Bsd, Funakoshi). Bsd-resistant colonies were picked up and expanded. Correctly targeted ES clones were confirmed by Southern blotting. For the *Rosa-M2rtTA/Col1a1*::*tetO-EWS-FLI1* system, the *EWS-FLI1-FLAG-HA-ires-mCherry-pA* sequence was inserted into pBS31, which was electropolated into KH2 ESCs as described previously (Beard et al., 2006). In both systems, chimeric mice were obtained by blastocyst injection.

Lentivirus vector construction, lentivirus infection and cell culture

To construct the doxycycline inducible lentiviral vector, we modified pEN-TmiRC3 and pSLIK-Neo lentiviral vector plasmids obtained from Addgene. First, pEN-TmiRC3 was digested with SpeI and XhoI to ligate *EWS-FLI1-FLAG-HA* downstream of the tetOP-mCMV promoter. Subsequently, the *ires-NeoR* cassette was ligated at the 3' of HA tag, followed by the excision of the *UbiC-rtTA3-ires-NeoR* sequence from pSLIK-Neo. After LR recombination between pEN-TmiRC3 (*tetO-EWS-FLI1-ires-Neo*) and pSLIK (without *UbiC-rtTA3-ires-Neo*), we obtained the pSLIK-*TetO-EWS-FLI1-ires-Neo* vector.

Bone marrow stromal cells were obtained from *Rosa26-M2rtTA* mice (Beard et al., 2006) at 3-4 weeks of age as reported previously (Soleimani and Nadri, 2009). At 3-4 days after the harvesting of bone marrow cells, non-adherent cells (hematopoietic cells) were removed by changing the culture media, and the adherent cells were infected with lentivirus. The cells were then cultured with DMEM (Nacalai) containing 10% FBS (Gibco), penicillin, streptomycin, 200 μg/ml G418 (Nacalai) and 2 μg/ml Dox (Sigma) for 2 months, and *EWS-FLI1*-dependent immortalized cells were established. Osteosarcoma cell lines, SCOS#2 and SCOS#12, were maintained in the same medium.

Single cell cloning

Single cell sorting of SCOS#2 and SCOS#12 cells was performed by FACS (Aria II, BD) in 96-well culture plates. Each sorted cell was cultured and expanded with Dox- and G418-containing

medium.

Cell growth assay

Sarcoma cells and ESCs/iPSCs were plated into 12 well culture plates at a density of 5×10^4 cells/well and 1×10^5 cells/well, respectively. The experiment was performed in triplicate, and each sample was measured twice. The number of cells was measured by an automatic cell counter (TC10^{TM}, Bio-Rad).

Xenograft assay

A total of 3×10^6 *EWS-FLI1*-dependent immortalized cells, *EWS-FLI1*-dependent sarcoma cells or ESCs/iPSCs were transplanted to NOD/ShiJic-scid Jcl mice or BALB/cSLC-nu/nu mice purchased from CLEA Japan and Japan SLC, respectively. *EWS-FLI1*-dependent immortalized cells were inoculated into NOD/ShiJic-scid Jcl mice, which were sacrificed at 10 weeks after the transplantation. *EWS-FLI1*-dependent osteosarcoma cells were inoculated into the subcutaneous tissue of BALB/cSLC-nu/nu mice. The tumor size was measured with digital calipers every week, and tumor volume was calculated as follows: volume = width$^2\times$length$\div$2. ESCs/iPSCs were transplanted into BALB/cSLC-nu/nu mice, and teratomas were obtained after 3-4 weeks.

RT-PCR and real-time quantitative RT-PCR

RNA was extracted using RNeasy Plus Mini Kit (QIAGEN). Up to 1 μg RNA was used for the reverse transcription reaction into cDNA. RT-PCR and real-time quantitative PCR were performed using Go-Taq Green Master Mix and Go-Taq qPCR Master Mix (Promega), respectively. Transcript levels were normalized by β-actin. PCR primers are available in Table S4.

Western blot analysis

Cultured cells were harvested in 500 μl of RIPA lysis buffer, and protein concentration was measured. Proteins were denatured with 2×SDS in 95 ℃ for 5 min. A total of 20 μg denatured protein was applied to 10% SDS/PAGE gel and transferred to PVDF membrane (Amersham Hybond-P PVDF Membrane, GE HealthCare). Proteins were detected by immunoblotting with anti-HA (Cell Signaling, C29F4, #3724; dilution 1:600) and anti-β actin (Santa Cruz, C4, sc-47778; dilution 1:1000) antibodies. Pierce ECL plus Western Blotting Substrate (Thermo Scientific) was used for visualization, and LAS4000 (GE HealthCare) was used for detection.

Histological analysis and immunohistochemistry

All tissue and tumor samples were fixed with 4% paraformaldehyde overnight and embedded in paraffin. Sections were stained with hematoxylin and eosin using standard protocol. For immunohistochemistry, the antibodies used were anti-HA (Cell signaling, C29F4, #3724; dilution 1:200) and anti-Ki67 (Abcam, SP6, ab16667; dilution 1:150).

Immunocytochemistry

Cultured cells were washed with PBS and fixed with 2% paraformaldehyde for 10 min at room temperature. For immunocytochemistry, antibodies used were anti-p53 (Abcam, PAb240, ab26; dilution 1:200) and anti-p21 (Abcam, HUGO291, ab107099; dilution 1:500).

ALP staining

Cultured cells were washed with PBS, fixed and stained with ALP Staining Kit (Sigma) according to the manufacturer's protocol.

Senescence-associated β -gal staining

Cultured cells were washed with PBS, fixed and stained with Senescence β-galactosidase Staining Kit (#9860S, Cell Signaling) according to the manufacturer's protocol.

Alizarin red staining

Cultured cells were washed with PBS and fixed with 4% paraformaldehyde for 5 min at room temperature. Fixed cells were washed with de-ionized water several times and stained in Alizarin red staining solution for 5 min (Alizarin red (Sigma, A5533) 2%, pH4.2 adjusted with NH_4OH). Similarly, de-paraffinized sections were stained in Alizarin red staining solution for 5 min.

Oil red O staining

Cultured cells were washed with PBS and fixed with 4% paraformaldehyde for 10 min at room temperature. Fixed cells were washed with 60% iso-propanol for 1 min and stained in oil red staining solution for 10 min (Oil red O (Sigma, O0625) 0.18% with 60% iso-propanol).

Detection of lentivirus integration site

We explored lentivirus integration sites as previously described with slight modifications (Varas et al., 2009). Extracted genomic DNA from SCOS#2 was digested into 500-800 bp fragments with

an ultrasonicator (Covaris E210). The linker-cassette obtained from annealing LC1 and LC2 was attached to the digested genomic DNA fragments. Subsequently, the first PCR was performed with AP1_F and pSLIK1_R primer set, followed by a nested PCR with AP2_F and pSLIK2_R primer set. PCR products were cloned to the pCR4-TOPO vector (Invitrogen) by the TA cloning method, and DNA sequences of the inserted fragments were analyzed by 3500xL Genetic Analyzer (Applied Biosystems) with seq_LTR_R primer. The obtained sequences were explored in at the BLAST website (http://blast.ncbi.nlm.nih.gov/Blast.cgi).

Bisulfite genomic sequencing

Bisulfite treatment was performed using the EZ DNA Methylation-Gold Kit^{TM} (ZYMO RESEARCH) according to the manufacturer's protocol. The PCR primers used are shown in Supplemental information. Amplified products were cloned into the pCR4-TOPO vector (Invitrogen) and transformed into DH5α. Colonies were randomly selected and sequenced with M13 forward and reverse primers for each gene.

ChIP-seq analysis

ChIP (Formaldehyde-Assisted Isolation of Regulatory Elements) was performed as described previously (Arioka et al., 2012). Anti-HA antibody (Nacalai, HA124, 06340-54) was used for the ChIP-seq analysis. Sequencing libraries were generated using TruSeq ChIP Sample Prep Kit (Illumina), assessed on an Agilent Bioanalyzer and quantified with KAPA Library Quantification Kits (KAPA BIOSYSTEMS). The libraries were sequenced to generate single-end 100 bp reads using Illumina MiSeq. We analyzed ChIP-seq data by mapping the reads using Bowtie2. The sequencing reads were aligned to mouse genome build mm9. We used the MACS (Zhang et al., 2008) version 1.4.2 peak finding algorithm to identify regions of ChIP-seq enrichment over background with p value 1×10^{-3}. To analyze and visualize the mapped reads, ngsplot was used (Shen et al., 2014). The motif analysis was performed using HOMER (Hypergeometric Optimization of Motif EnRichment) software (Heinz et al., 2010).

Exome analysis and direct sequencing

Genomic DNA of SCOS#2-A1, sarcoma iPSC#2-A1 and sarcoma-iPSC#2-A1-derived secondary sarcoma was extracted with PureLink® Genomic DNA Mini Kit (Invitrogen). Whole-exome capture was done with the SureSelect XT (Agilent Technologies). The exome libraries were then sequenced on a HiSeq2500 (Illumina). Raw sequencing reads were mapped to the mouse reference genome (mm10) using the Burrows-Wheeler Aligner (bwa-0.7.12) and were processed with SAMtools (samtools-1.2). Genome

Analysis Toolkit (GATK version: 3.5) was used to perform base recalibration and local realignment. SNVs and indels were called by the GATK HaplotypeCaller. We selected somatic variants by removing SNPs and indels reported in the mm10 (VCF file was downloaded from NCBI) and by removing the overlapping variants present in 129S1/Sv exome data (SRP007328). Remaining variants were annotated by SnpEff version 4.2 using RefGene GRCm38.82. To this end, we detected 15567, 16221 and 15338 variants including 577, 620 and 554 missense mutations in SCOS#2-A1, sarcoma iPSC#2-A1 and the secondary sarcoma, respectively. 405 missense mutations were overlapped in SCOS#2-A1, sarcoma iPSC#2-A1 and the secondary sarcoma. In order to extract unique mutations to this sarcoma model, the missense mutations were further compared with exome data of other tumor models (colon tumor and clear cell sarcoma model; submitted). A list of the unique mutations was shown in Table S2. For direct sequencing analysis, the PCR product containing the mutation candidate site was sequenced with the genetic analyzer ABI 3500xL (Applied Biosystems).

Supplemental References

Arioka, Y., Watanabe, A., Saito, K., and Yamada, Y. (2012). Activation-induced cytidine deaminase alters the subcellular localization of Tet family proteins. PLoS One *7*, e45031.

Beard, C., Hochedlinger, K., Plath, K., Wutz, A., and Jaenisch, R. (2006). Efficient method to generate single-copy transgenic mice by site-specific integration in embryonic stem cells. Genesis *44*, 23-28.

Feng, Y., Sassi, S., Shen, J.K., Yang, X., Gao, Y., Osaka, E., Zhang, J., Yang, S., Yang, C., Mankin, H.J.*, et al.* (2015). Targeting CDK11 in osteosarcoma cells using the CRISPR-Cas9 system. J Orthop Res *33*, 199-207.

Grilli, A., Sciandra, M., Terracciano, M., Picci, P., and Scotlandi, K. (2015). Integrated approaches to miRNAs target definition: time-series analysis in an osteosarcoma differentiative model. BMC Med Genomics *8*, 34.

Heinz, S., Benner, C., Spann, N., Bertolino, E., Lin, Y.C., Laslo, P., Cheng, J.X., Murre, C., Singh, H., and Glass, C.K. (2010). Simple combinations of lineage-determining transcription factors prime cis-regulatory elements required for macrophage and B cell identities. Mol Cell *38*, 576-589.

Kawano, M., Tanaka, K., Itonaga, I., Ikeda, S., Iwasaki, T., and Tsumura, H. (2015). microRNA-93 promotes cell proliferation via targeting of PTEN in Osteosarcoma cells. J Exp Clin Cancer Res *34*, 76.

Lu, J., Song, G., Tang, Q., Zou, C., Han, F., Zhao, Z., Yong, B., Yin, J., Xu, H., Xie, X.*, et al.* (2015). IRX1 hypomethylation promotes osteosarcoma metastasis via induction of CXCL14/NF-κB signaling. J Clin Invest *125*, 1839-1856.

Mackintosh, C., Ordóñez, J.L., García-Domínguez, D.J., Sevillano, V., Llombart-Bosch, A., Szuhai, K., Scotlandi, K., Alberghini, M., Sciot, R., Sinnaeve, F.*, et al.* (2012). 1q gain and CDT2 overexpression underlie an aggressive and highly proliferative form of Ewing sarcoma. Oncogene *31*, 1287-1298.

Miyagawa, Y., Okita, H., Nakaijima, H., Horiuchi, Y., Sato, B., Taguchi, T., Toyoda, M., Katagiri, Y.U., Fujimoto, J., Hata, J.*, et al.* (2008). Inducible expression of chimeric EWS/ETS proteins confers Ewing's family tumor-like phenotypes to human mesenchymal progenitor cells. Mol Cell Biol *28*, 2125-2137.

Ohta, S., Nishida, E., Yamanaka, S., and Yamamoto, T. (2013). Global splicing pattern reversion during somatic cell reprogramming. Cell Rep *5*, 357-366.

Shen, L., Shao, N., Liu, X., and Nestler, E. (2014). ngs.plot: Quick mining and visualization of next-generation sequencing data by integrating genomic databases. BMC Genomics *15*, 284.

Soleimani, M., and Nadri, S. (2009). A protocol for isolation and culture of mesenchymal stem cells from mouse bone marrow. Nat Protoc *4*, 102-106.

Takigami, I., Ohno, T., Kitade, Y., Hara, A., Nagano, A., Kawai, G., Saitou, M., Matsuhashi, A., Yamada, K., and Shimizu, K. (2011). Synthetic siRNA targeting the breakpoint of EWS/Fli-1 inhibits growth of

Ewing sarcoma xenografts in a mouse model. Int J Cancer *128*, 216-226.

Ullah, M., Sittinger, M., and Ringe, J. (2014). Transdifferentiation of adipogenically differentiated cells into osteogenically or chondrogenically differentiated cells: phenotype switching via dedifferentiation. Int J Biochem Cell Biol *46*, 124-137.

Varas, F., Stadtfeld, M., de Andres-Aguayo, L., Maherali, N., di Tullio, A., Pantano, L., Notredame, C., Hochedlinger, K., and Graf, T. (2009). Fibroblast-derived induced pluripotent stem cells show no common retroviral vector insertions. Stem Cells *27*, 300-306.

Zhang, Y., Liu, T., Meyer, C.A., Eeckhoute, J., Johnson, D.S., Bernstein, B.E., Nusbaum, C., Myers, R.M., Brown, M., Li, W.*, et al.* (2008). Model-based analysis of ChIP-Seq (MACS). Genome Biol *9*, R137.